





## RESEARCH ARTICLE

# Morphology of the *Homo naledi* femora from Lesedi

Christopher S. Walker<sup>1,2,3</sup>  | Zachary D. Cofran<sup>4,3</sup> | Mark Grabowski<sup>5</sup> |  
 Damiano Marchi<sup>6,3</sup> | Rebecca W. Cook<sup>1,2</sup> | Steven E. Churchill<sup>2,3</sup> |  
 Kimberleigh A. Tommy<sup>7,3</sup> | Zachary Throckmorton<sup>8,3</sup> | Ann H. Ross<sup>9</sup> |  
 John Hawks<sup>10,3</sup>  | Gabriel S. Yapuncich<sup>1,2</sup>  | Adam P. Van Arsdale<sup>11</sup> |  
 Frederika I. Rentzeperis<sup>12</sup> | Lee R. Berger<sup>3</sup>  | Jeremy M. DeSilva<sup>12,3</sup>

<sup>1</sup>Department of Molecular Biomedical Sciences, College of Veterinary Medicine, North Carolina State University, Raleigh, North Carolina

<sup>2</sup>Department of Evolutionary Anthropology, Duke University, Durham, North Carolina

<sup>3</sup>Evolutionary Studies Institute, University of the Witwatersrand, Johannesburg, South Africa

<sup>4</sup>Anthropology Department, Vassar College, Poughkeepsie, New York

<sup>5</sup>Research Centre in Evolutionary Anthropology and Palaeoecology, School of Natural Sciences and Psychology, Liverpool John Moores University, Liverpool, UK

<sup>6</sup>Department of Biology, University of Pisa, Pisa, Italy

<sup>7</sup>Human Variation and Identification Research Unit, School of Anatomical Sciences, University of the Witwatersrand, Johannesburg, South Africa

<sup>8</sup>Department of Anatomy, Arkansas College of Osteopathic Medicine, Fort Smith, Arkansas

<sup>9</sup>Department of Biological Sciences, North Carolina State University, Raleigh, North Carolina

<sup>10</sup>Department of Anthropology, University of Wisconsin, Madison, Wisconsin

<sup>11</sup>Department of Anthropology, Wellesley College, Wellesley, Massachusetts

<sup>12</sup>Department of Anthropology, Dartmouth College, Hanover, New Hampshire

## Correspondence

Christopher S. Walker, Department of Molecular Biomedical Sciences, College of Veterinary Medicine, North Carolina State University, Raleigh, NC.  
 Email: christopher\_walker@ncsu.edu

## Funding information

University of the Witwatersrand; National Research Foundation; National Geographic Society

## Abstract

**Objectives:** The femoral remains recovered from the Lesedi Chamber are among the most complete South African fossil hominin femora discovered to date and offer new and valuable insights into the anatomy and variation of the bone in *Homo naledi*. While the femur is one of the best represented postcranial elements in the *H. naledi* assemblage from the Dinaledi Chamber, the fragmentary and commingled nature of the Dinaledi femoral remains has impeded the assessment of this element in its complete state.

**Materials and methods:** Here we analyze and provide descriptions of three new relatively well-preserved femoral specimens of *H. naledi* from the Lesedi Chamber: U.W. 102a-001, U.W. 102a-003, and U.W. 102a-004. These femora are quantitatively and qualitatively compared to multiple extinct hominin femoral specimens, extant hominid taxa, and, where possible, each other.

**Results:** The Lesedi femora are morphologically similar to the Dinaledi femora for all overlapping regions, with differences limited to few traits of presently unknown significance. The Lesedi distal femur and mid-diaphysis preserve anatomy previously unidentified or unconfirmed in the species, including an anteroposteriorly expanded midshaft and anteriorly expanded patellar surface. The hypothesis that the Lesedi femoral sample may represent two individuals is supported.

**Discussion:** The Lesedi femora increase the range of variation of femoral morphology in *H. naledi*. Newly described features of the diaphysis and distal femur are either taxonomically uninformative or *Homo*-like. Overall, these three new femora are consistent with previous functional interpretations of the *H. naledi* lower limb as belonging to a species adapted for long distance walking and, possibly, running.

**KEYWORDS**

bipedal locomotion, hominin, Rising Star, thigh

## 1 | INTRODUCTION

To date, 1,681 fossil elements attributed to *Homo naledi* have been reported from the Rising Star cave system (Berger et al., 2015; Hawks et al., 2017), including 32 femoral elements. Twenty-nine of these femoral elements recovered from the Dinaledi Chamber have been described previously (Berger et al., 2015; Marchi et al., 2017). The Dinaledi femora, dated to between 335 and 236 kya (Dirks et al., 2017), evince a mosaic of primitive (*Australopithecus*-like), shared derived (*Homo*-like), and autapomorphic features. Their long, superoinferiorly tall, and anteroposteriorly compressed femoral necks, that are anteverted relative to platymeric proximal diaphyses, and thick diaphyseal cortices are *Australopithecus*-like in nature (Marchi et al., 2017). Prominent and posteriorly positioned gluteal tuberosities and well-defined lineae asperae are among the distinctly *Homo*-like traits of the Dinaledi femora (Marchi et al., 2017). Notably, a mediolaterally-elongated depression on the superior aspect of the neck and two associated parallel ridges of bone are unique to *H. naledi* (Marchi et al., 2017). In combination with the rest of the Dinaledi lower limb material, the femoral morphology is compatible with a fully bipedal gait (Harcourt-Smith et al., 2015; Marchi et al., 2017). Beyond this, the adaptive and evolutionary significance of the unique suite of femoral features of *H. naledi* is currently unknown.

Here we describe three femoral elements recently recovered from the Lesedi Chamber of the Rising Star cave system and attributed to *H. naledi* (Hawks et al., 2017): U.W. 102a-001, U.W. 102a-003, and U.W. 102a-004 (Figure 1). Through comparative analysis, we demonstrate that the Lesedi distal femur and mid-diaphysis reveal a largely *Homo*-like suite of features which contrast with the more anatomically mosaic proximal end.

## 2 | MATERIALS AND METHODS

### 2.1 | Comparative sample

The comparative samples used in analyses herein include femora from three extant species (*Homo sapiens*, *Pan troglodytes*, and *Gorilla gorilla*) and fossil femora attributed to multiple taxa, including *Australopithecus africanus*, *Australopithecus afarensis*, *Australopithecus sediba*, robust *Australopithecus (Paranthropus) spp.*, *Homo erectus sensu lato* (with Early Pleistocene *Homo sp. indet.*), and *H. naledi* from Dinaledi. Details, including



**FIGURE 1** Posterior view of the three femoral fragments of *H. naledi* from the Lesedi Chamber. Partial left femur (image left) comprised of U.W. 102a-003 (proximal) and U.W. 102a-004 (distal). Partial right femur (image right) represented by U.W. 102a-001. Scale bar = 5 cm

sample sizes, composition, origins, and individual fossil identification codes can be found in Table 1.

## 2.2 | Measurements and data collection

Measurements of the femur used in this study (Figure 2) include maximum superoinferior (SI) head diameter (FHD), minimum SI neck diameter (height; NH; taken orthogonal to the long axis of the neck), anteroposterior (AP) neck diameter (breadth; NB; taken orthogonal to

NH), neck-shaft angle (NSA), neck length (NL; maximum length from the lateral-most edge of the femoral head to the intertrochanteric crest), subtrochanteric mediolateral (ML) diameter (SML; maximum ML diameter of the proximal diaphysis taken just distal to the level of the lesser trochanter), subtrochanteric AP diameter (SAP; taken orthogonal to SML), and femoral neck anteversion angle (FNA). To evaluate femoral neck and subtrochanteric shape (or platymeric index), ratios of neck and subtrochanteric diameters were calculated as follows: neck shape = (neck AP/SI \* 100); platymeric

**TABLE 1** Comparative sample composition, sizes, origins, and individual fossil identification codes

Taxon	N (or fossil specimen ID)
<i>Homo sapiens</i>	295 (from <sup>a</sup> : PMAE, KSU, DC, NMNH, UI, TU, CMNH, DU, UT, NCSU, UM)
<i>Pan troglodytes</i>	42 (from <sup>a</sup> : MCZ, NMNH, CMNH, TU)
<i>Gorilla gorilla</i>	47 (from <sup>a</sup> : MCZ, NMNH, CMNH, TU)
<i>Australopithecus afarensis</i>	A.L. 128-1 <sup>b</sup> , A.L. 152-2 <sup>c</sup> , A.L. 211-1 <sup>d</sup> , A.L. 288-1 <sup>b,c,e</sup> , A.L. 333-3 <sup>c,d</sup> , A.L. 333-95 <sup>b,c,d</sup> , A.L. 333-131 <sup>d</sup> , A.L. 827-1 <sup>c</sup> , MAK-VP 1/1 <sup>f</sup> , A.L. 333-142 <sup>c</sup> , A.L. 333w-40 <sup>g</sup> , KSD-VP-1/1 <sup>h</sup>
<i>Australopithecus africanus</i>	MLD 17 <sup>i</sup> , MLD 25 <sup>j</sup> , MLD 46 <sup>k</sup> , Sts 14 <sup>b,j</sup> , StW 25 <sup>b</sup> , StW 31 <sup>i</sup> , StW 99 <sup>b</sup> , StW 179 <sup>b</sup> , StW 300 <sup>i</sup> , StW 311 <sup>b,i</sup> , StW 361 <sup>b</sup> , StW 392 <sup>b</sup> , StW 403 <sup>b</sup> , StW 431 <sup>i</sup> , StW 443 <sup>i</sup> , StW 479 <sup>b</sup> , StW 501 <sup>b</sup> , StW 522 <sup>b</sup> , StW 527 <sup>b</sup> , StW 598 <sup>m</sup>
Robust <i>Australopithecus</i> ( <i>Paranthropus</i> ) spp.	SK 14024 <sup>b</sup> , SK 3121 <sup>b</sup> , SK 3155B <sup>i</sup> , SK 50 <sup>j</sup> , SK 82 <sup>b</sup> , SK 97 <sup>b</sup> , SKW 19 <sup>b</sup> , SKX 3121 <sup>b</sup> , SWT1/LB-2 <sup>n</sup> , TM 1605 <sup>j</sup> , OH 20 <sup>b</sup> , OH 80-12 <sup>o</sup> , KNM-ER 1500d <sup>b</sup> , KNM-ER 1503 <sup>b</sup> , KNM-ER 1505 <sup>b</sup>
<i>Australopithecus sediba</i>	U.W. 88-51 (MH2) <sup>b</sup> , U.W. 88-4,5,39 (MH1) <sup>b</sup>
<i>Homo erectus</i> ( <i>ergaster</i> ) and <i>Homo sp. indet.</i> (Early Pleistocene)	BOU-VP-1/75 <sup>p</sup> , BOU-VP-19/63 <sup>p</sup> , BSN49/P2 <sup>q</sup> , D4167 <sup>a,r</sup> , D3901 <sup>q</sup> , KNM-WT 15000 <sup>b,s</sup> , KNM-ER 736 <sup>b</sup> , KNM-ER 737 <sup>b</sup> , KNM-ER 803A <sup>b</sup> , KNM-ER 1472 <sup>b</sup> , KNM-ER 1475 <sup>b</sup> , KNM-ER 1481 <sup>b</sup> , KNM-ER 1808 <sup>b</sup> , KNM-ER 3228 <sup>k</sup> , KNM-ER 5880A <sup>b</sup> , KNM-ER 5881 <sup>b</sup> , OH 28 <sup>b</sup> , OH 34 <sup>t</sup> , OH 62 <sup>b</sup>
<i>Homo naledi</i>	U.W. 101-002 <sup>b</sup> , U.W. 101-003 <sup>b</sup> , U.W. 101-012 <sup>b</sup> , U.W. 101-018 <sup>b</sup> , U.W. 101-143 <sup>b</sup> , U.W. 101-215 <sup>b</sup> , U.W. 101-268 <sup>b</sup> , U.W. 101-271 <sup>b</sup> , U.W. 101-341 <sup>b</sup> , U.W. 101-398 <sup>b</sup> , U.W. 101-421 <sup>b</sup> , U.W. 101-545 <sup>b</sup> , U.W. 101-857 <sup>b</sup> , U.W. 101-898 <sup>b</sup> , U.W. 101-1136 <sup>b</sup> , U.W. 101-1284 <sup>b</sup> , U.W. 101-1300 <sup>b</sup> , U.W. 101-1391 <sup>b</sup> , U.W. 101-1434 <sup>b</sup> , U.W. 101-1475 <sup>b</sup> , U.W. 101-1482 <sup>b</sup>
<i>Homo sp. indet.</i> (Middle and Late Pleistocene)	Berg Aukas <sup>b</sup> , KNM-ER 999 <sup>b</sup> , Kabwe E689 <sup>u</sup> , Kabwe E907 <sup>u</sup>

<sup>a</sup>Institutions: CMNH = Cleveland Museum of Natural History; DC: Dart Collection, University of the Witwatersrand; KSU = Kent State University Libben Paleoindivian collection; NCSU = North Carolina State University Forensic Analysis Lab Collection; NMNH = National Museum of Natural History (Smithsonian Institution) Terry Collection; PMAE = Merida and Mistihalj populations, Harvard Peabody Museum of Archeology and Ethnology; TU = Department of Anthropology, Tulane University; MCZ = Harvard Museum of Comparative Zoology; DU = Duke University; UI = Department of Anthropology, University of Iowa; UM = University of Michigan Anthropology Teaching Collection (unknown provenance); UT = University of Tennessee Dr. William M. Bass Collection.

<sup>b</sup>Data collected from original fossils or high quality casts by a study author or associated researcher.

<sup>c</sup>Data from Ward, Kimbel, Harmon, and Johanson (2012).

<sup>d</sup>Data from Lovejoy, Johanson, and Coppens (1982).

<sup>e</sup>Data from Johanson et al. (1982).

<sup>f</sup>Data from Lovejoy, Meindl, Ohman, Heiple, and White (2002).

<sup>g</sup>Data from McHenry (1988).

<sup>h</sup>Data from Haile-Selassie et al. (2010).

<sup>i</sup>Data from Jungers (1988).

<sup>j</sup>Data from Plavcan, Hammond, and Ward (2014).

<sup>k</sup>Data from Reed, Kitching, Grine, Jungers, and Sokoloff (1993).

<sup>l</sup>Data from McHenry (1992).

<sup>m</sup>Data from Partridge, Granger, Caffee, and Clarke (2003).

<sup>n</sup>Data from Pickering et al. (2012).

<sup>o</sup>Data from Domínguez-Rodrigo et al. (2013).

<sup>p</sup>Data from Gilbert (2008).

<sup>q</sup>Data from Ruff (2010).

<sup>r</sup>Data from Lordkipanidze et al. (2007).

<sup>s</sup>Data from Walker and Leakey (1993).

<sup>t</sup>Data from Haeusler and McHenry (2004).

<sup>u</sup>Data from Grine, Jungers, Tobias, and Pearson (1995).

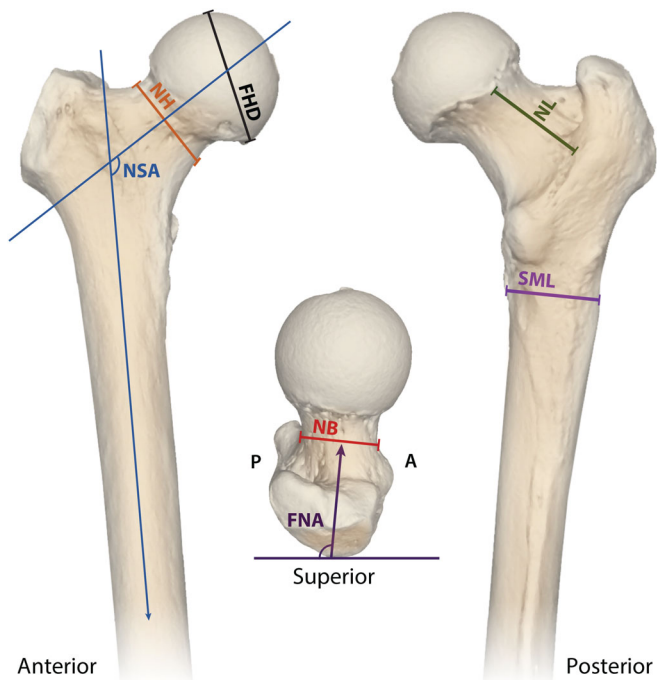


**FIGURE 2** Measurements of the femur. Maximum superoinferior head diameter (FHD), minimum superoinferior neck diameter (height; NH), anteroposterior neck diameter (breadth; NB), neck-shaft angle (NSA), neck length (NL), subtrochanteric mediolateral diameter (SML), subtrochanteric anteroposterior diameter (SAP; not pictured; taken orthogonal to SML), and femoral neck anteversion angle (FNA)

index = (subtrochanteric AP/ML \* 100). All linear measurements were taken using digital calipers on original specimens or high quality casts by study authors unless otherwise noted. NSA (defined here as the angle between the longitudinal axis of the femoral neck and the longitudinal axis of the femoral shaft) was taken with a handheld goniometer on the anterior aspect of the specimen, while FNA (defined here as the angle between the longitudinal axis of the femoral neck and the sagittal plane) was taken following Marchi et al. (2017, pp. 3–4 and Figures 1 and 2). Femoral neck shape was also qualitatively evaluated via assessment of periosteal contours (or external outline) of cross-sections (transverse plane; perpendicular to the long axis of the femoral neck) at the neck-shaft junction. Femora were surface scanned using an Artec Spider blue light scanner (100  $\mu\text{m}$  resolution, 30  $\mu\text{m}$  accuracy) and cross-sections were digitally extracted using Geomagic Design X (3D Systems, 2015).

### 2.3 | Reconstructions and measurement estimations

Damage to the head and neck of U.W. 102a-001 precludes an accurate measurement of both FHD and NB on this specimen. The head is heavily abraded on nearly all surfaces and the anterosuperior aspect of the neck is broken, such that at least one measurement point falls on exposed trabeculae (see fossil descriptions for further details). To facilitate comparisons with Dinaledi and other fossil hominin femora, we used Geomagic Design X (3D Systems, 2015) to digitally estimate

FHD and reconstruct the missing periosteal border of the anterior neck of U.W. 102a-001 to estimate NB.

Reconstruction of the anterior femoral neck (Figure 3) focused specifically on the level of NH, since it is at this level that NB is taken (orthogonal to NH). Transverse sections (cross-sections) were digitally extracted from the U.W. 102a-001 3D mesh at 1 mm intervals along the entire length of the femoral neck. The cross-section at the level of NH (i.e., the section of interest; SOI) was identified using physical landmarks and confirmed with a digital measurement of NH matching the instrumentally determined value (24.4 mm). Adjacent sections were stacked on the SOI to evaluate overlapping and non-overlapping regions of preserved cortical bone. One section, 2 mm lateral to the SOI, preserved more of the anteroinferior periosteal contour than the SOI and curvature of this portion was consistent with the preserved, connecting section of the SOI contour. Accordingly, the portion of partially-overlapping periosteal border from the adjacent section was merged with the SOI. To estimate the rest of the missing contour, the SOI was compared to corresponding sections in the Dinaledi femoral sample. While no Dinaledi femoral neck transverse section closely matched U.W. 102a-001 in overall shape, one – U.W. 101-398 – possessed an anterior/anterosuperior border that seamlessly adjoined the broken borders of the SOI anterior contour, when it was scaled to match U.W. 102a-001 in size, mirrored, and slightly rotated. This section of U.W. 101-398 was cut and placed on the SOI creating a composite cross-section. The composite section was then stitched and re-measured, yielding an estimated AP diameter (NB) of 17.5 mm.

Estimation of U.W. 102a-001 FHD utilized a sphere-fitting technique incorporating preserved subchondral surfaces (Figure 4; cf., Hammond, Plavcan, & Ward, 2013; Plavcan et al., 2014; Ward et al., 2015). This procedure was undertaken in Geomagic Design X (3D Systems, 2015) using the sphere-fitting function, which applies a best-fit sphere to selected surfaces. The preserved subchondral areas were identified on a 3D mesh of the specimen, by both inspecting a 3D print and creating a curvature map in Amira 6.4 (ThermoFisher Scientific, 2017). U.W. 102a-001 preserves three subchondral surfaces: one roughly rectangular patch measuring 196  $\text{mm}^2$  located on the posterior aspect of the head (Figure 4), and two smaller and more irregularly-shaped patches adjacent (one inferomedial and one superolateral) to the large patch (Figure S1). Care was taken to select only smooth subchondral surface and to avoid areas of breakage. Spheres were fitted to all preserved subchondral surfaces (estimated FHD 36.4 mm) and to only the largest and most precisely defined patch (estimated FHD 35.5 mm). Hereafter, we consider the average diameter of these two reconstructions, 36.0 mm, as the estimated FHD for U.W. 102a-001.

In order to assess the error of this estimated FHD, we compared empirical and sphere-fitted diameters (cf. Hammond et al., 2013) in a subset of our comparative sample, focusing solely on the femoral heads of *H. sapiens* ( $n = 28$ , mixed-sex, from the Bass Collection, University of Tennessee, Knoxville) and fossil hominins ( $n = 10$ ; A.L. 288-1, KNM-ER 1481, KNM-ER 1503, SK 82, SK 97, StW 99, KNM-WT 15000, Berg Aukas, Kabwe E689, Kabwe E907). Comparative specimens were digitized using the same equipment used to

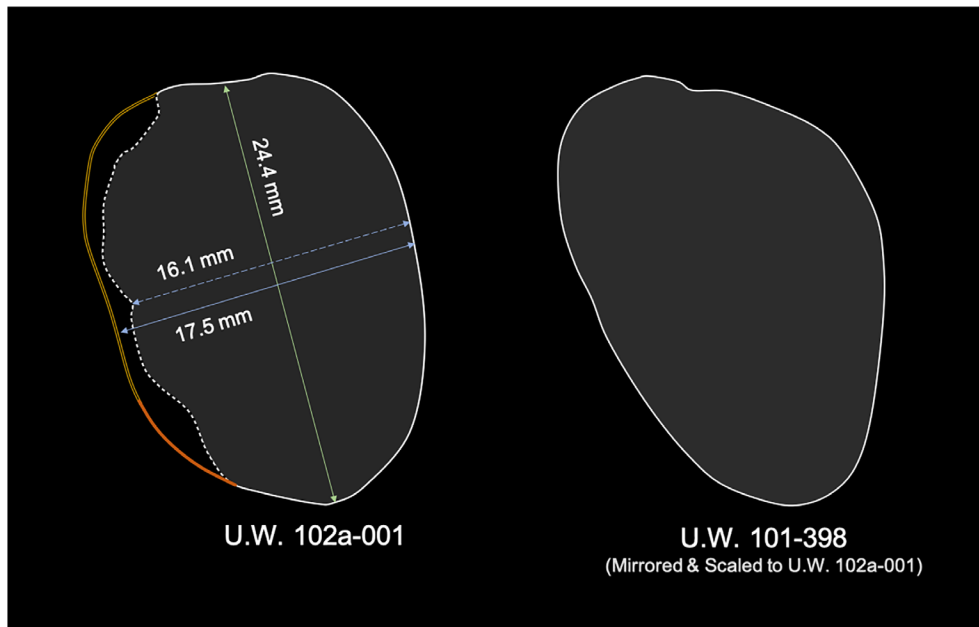


**FIGURE 3** Transverse sections of the U.W. 102a-001 and U.W. 101-398 femoral necks at the level of minimum superoinferior neck diameter. The missing periosteal border the anterior neck of U.W. 102a-001, at the level of interest, was reconstructed using a combination of patterning on an equivalent section from Dinaledi specimen U.W. 101-398 and a proximate U.W. 102a-001 transverse neck section. The solid white lines define areas of preserved cortical bone/periosteal borders. The dotted white line represents the area of breakage (exposed trabeculae). The solid orange line is a periosteal border segment reconstructed by overlaying a transverse neck section from U.W. 102a-001 taken 2 mm lateral to the section of interest, for which the contours of each section match anteroinferiorly. The split yellow line represents a periosteal border created by overlaying a mirrored, scaled, and slightly rotated U.W. 101-398, adjusted to accommodate minute variation in the curvature of preserved periosteal border of U.W. 102a-001, both anterosuperiorly and anteroinferiorly

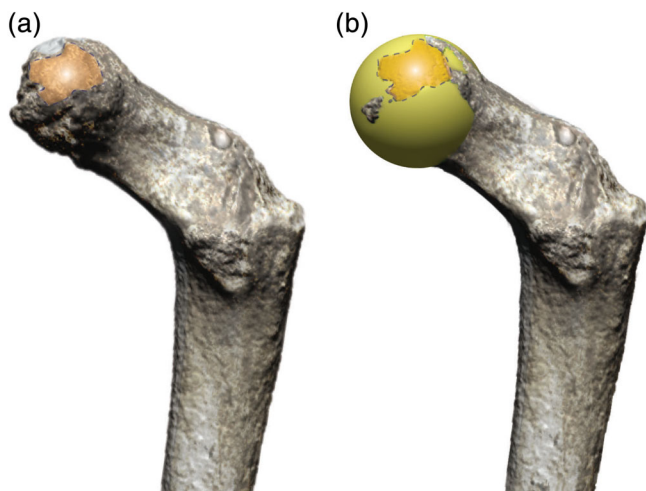


**FIGURE 4** U.W. 102a-001 femoral head sphere-fitting. 3D mesh of U.W. 102a-001 in posterior view. (a) The largest continuous patch of preserved subchondral is highlighted in orange. (b) Sphere (yellow) fitted to the highlighted surface

acquire Lesedi femoral 3D meshes (Artec Spider blue light scanner), and spheres were fitted following the same procedures and software used to reconstruct U.W. 102a-001. Because of the irregular shape and somewhat ambiguous positioning of the preserved subchondral surfaces of U.W. 102a-001, it is difficult to isolate a clearly homologous surface on individuals within the comparative samples.

Therefore, for each comparative specimen, we tried to replicate the size and position of only the largest subchondral patch on U.W. 102a-001. Each individual was measured three times, and the average value was then compared to empirical superoinferior FHD using least squares regression in R software (R Core Team, 2018). We assessed the performance of the sphere estimates with three measures: residual standard error (*RSE*) and the coefficient of determination ( $R^2$ ) from the linear model, and percent prediction error (*PPE*). *RSE* and  $R^2$  were automatically calculated as part of the regression analysis in R. *PPE* was calculated as the absolute difference between empirical FHD and sphere-fitted FHD, divided by empirical FHD; this is “*PPE2*” of Hammond et al. (2013). Regressions and *PPE* were calculated separately for *H. sapiens* only, fossil hominins only, and the combined human and fossil hominin sample (Tables 2 and 3).

## 2.4 | Discriminant function analysis

A linear discriminant function analysis (DFA) was used to assess broad morphological affinities and differences of the Lesedi proximal femur relative to other hominin groups. U.W. 102a-001 was entered as an unknown alongside *H. sapiens* ( $n = 58$ , mixed-sex, from the University of Michigan Department of Anthropology teaching collection and the Merida and Mistihalj skeletal collections at the Harvard Peabody Museum of Archeology and Ethnology), *Australopithecus* (A.L. 288-1, A.L. 333-3, OH 20, KNM-ER 1503, MH 1, SK 82, SK 97), fossil *Homo*

SI diameter	Intercept	Slope	RSE	R <sup>2</sup>	Lesedi mean estimate
<i>H. sapiens</i>	5.29	0.86	1.31	0.92	36.31
SE	2.40	0.05			
t-value	2.20	16.92			
p value	<b>0.04</b>	<b>&lt;0.01</b>			
Fossil hominins	3.19	0.93	1.54	0.98	36.74
SE	2.20	0.05			
t-value	1.45	18.01			
p value	0.20	<b>&lt;0.01</b>			
All	4.66	0.88	1.41	0.95	36.25
SE	1.56	0.03			
t-value	2.99	26.01			
p value	<b>0.01</b>	<b>&lt;0.01</b>			

**TABLE 2** Regression results comparing empirical versus fitted sphere FHD for *H. sapiens* and fossil hominins

Bold values indicate statistical significance at  $p \leq 0.05$ .

**TABLE 3** Estimated FHD for U.W. 102a-001 using mean prediction errors for *H. sapiens* and fossil hominins

Sample	Mean PPE (%)	Lesedi sphere estimate (mm)	Min. estimated diameter (mm)	Max. estimated diameter (mm)
<i>H. sapiens</i>	3.4	36.0	34.8	37.2
Fossil hominins	3.1	36.0	34.9	37.1
All	3.3	36.0	34.8	37.2

(KNM-ER 1472, KNM-ER 1481, KNM-WT 15000, LB1), and *H. naledi* from Dinaledi (U.W. 101-002, U.W. 101-398, U.W. 101-1391). This DFA (calculated in IBM SPSS Statistics Version 20) is an amended version of the DFA presented in Marchi et al. (2017) and includes five linear metrics (FHD, NB, SAP, SML, and NL) which were size-adjusted by dividing each variable by the geometric mean of all five metrics (Mosimann, 1970; Richmond & Jungers, 2008). To evaluate the performance of the DFA with respect to group classification accuracy, cross-validation tests were performed (IBM SPSS Statistics Version 20).

## 2.5 | Bilateral asymmetry

Hawks et al. (2017) argued that a minimum of two adult individuals are present within the Lesedi Chamber assemblage based on mandibular and dental remains. The two proximal femoral elements, U.W. 102a-001 and U.W. 102a-003, are morphologically different from one another in ways that suggest they may not be antimeres and, therefore, Hawks et al. (2017) accepted that these specimens may represent two different adult individuals (albeit two individuals with similarly-sized femora). Here, we test the hypothesis that the size variation between these two specimens is consistent with bilateral asymmetry within a single adult individual. To quantitatively assess this, U.W. 102a-001 and U.W. 102a-003 were evaluated in the context of 51 mixed-sex modern human femoral left/right pairs (from the

University of Michigan Department of Anthropology teaching collection). Though hip biomechanics may differ between species, influencing subtrochanteric dimensions differently, *H. sapiens* are the best available extant proxy to examine bilateral asymmetry in an extinct biped like *H. naledi*. First, variation (% difference) between U.W. 102a-001 and U.W. 102a-003 subtrochanteric dimensions was compared to bilateral asymmetry in the modern human sample. Secondly, we used exact randomization sampling methods (Manly, 2006; Sokal & Rohlf, 1995) to determine the probability of drawing two femora as different (with respect to subtrochanteric dimensions) as U.W. 102a-001 and U.W. 102a-003 from a mixed human sample (all possible left/right pairings). This approach was used because exact randomization sampling allows for probability computations with small sample sizes and is free of the assumption that data are normally distributed (Manly, 2006; Richmond & Jungers, 1995).

## 3 | RESULTS

### 3.1 | Descriptions

U.W. 102a-001 (Figure 5) is a proximal right femur measuring 163.8 mm SI from the superior aspect of the eroded femoral head to a jagged break in the diaphysis, distally. Only a small portion of the posterior subchondral surface of the femoral head is preserved, but it is badly eroded on the superior, inferior, and (especially) anterior aspects. The preserved SI height of the femoral head is 30.4 mm and the estimated SI diameter is 36.0 mm (see Section 3.2). The anterosuperior neck is broken and missing, with partially sediment infilled trabecular bone exposed from the anterior head, medially, to the base of the greater trochanter, laterally. The intact portion of the anteroinferior neck is smooth, showing no clear sign of an intertrochanteric line. The inferior and posterior aspects of the neck are well-preserved. An indistinct obturator externus groove is present, running inferomedial to superolateral near the midpoint of the posterior neck. Some cortical bone is preserved on the most superior aspect of the neck, which allows for minimum SI neck height (24.4 mm) to be

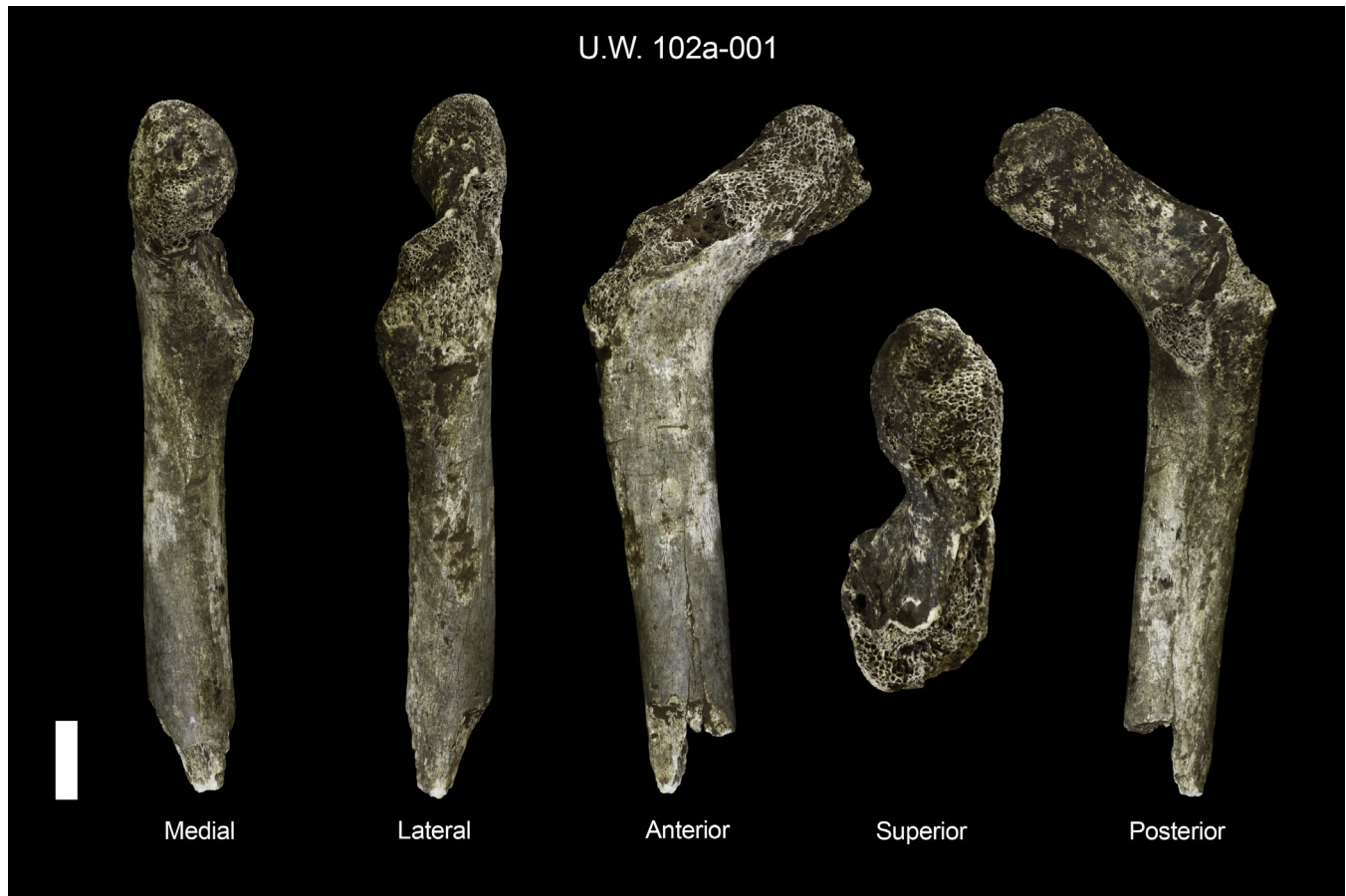


**FIGURE 5** Partial right proximal femur U.W. 102a-001. Scale bar = 2 cm

measured with reasonable accuracy. The AP width of the neck (orthogonal to SI) measures 16.1 mm, but the anterior point of this measurement is on exposed trabeculae and is, thus, an underestimate. The anteroposterior neck width is estimated to be 17.5 mm (see Section 3.2). The neck is 33.9 mm long from the most lateral aspect of the head (at the head-neck border) to the small remnant of the intertrochanteric crest. The greater trochanter is broken and missing, with the exception of a small portion of its distolateral surface. A pit, possibly for the attachment of the conjoined tendon of obturator internus and the gemelli, is present on the most lateral aspect of the preserved superoposterior neck, but it is small and not notably mediolaterally expanded. Above this pit, there is a weakly defined mediolateral-oriented bony pillar which is consistent with the inferoposterior pillar described for the Dinaledi femora (Marchi et al., 2017). The combination of damage to the greater trochanter and femoral neck preclude assessment of the superoanterior neck pillar, which is found in all femora of *H. naledi* from Dinaledi (Marchi et al., 2017). The lesser trochanter is sheared off at its base, exposing a 15.1 mm SI by 15.9 mm ML patch of trabecular bone. Immediately superior to the lesser trochanter is an ~2.5 mm diameter hole positioned superoinferiorly, boring deep to the lesser trochanter. The diaphysis is, overall, well-preserved, though there is notable and pervasive longitudinally-oriented cracking (consistent with postmortem drying) and other superficial damage. At

the level of the lesser trochanter, just inferior to the missing greater trochanter on the lateral shaft, is a pronounced, anteroposteriorly-oriented defect measuring 10.6 mm by 2.3 mm. Distal to this defect on the lateral diaphysis is an irregularly-shaped shallow depression in the cortical bone that is sediment infilled. Adjacent to this depression, on the lateral, anterolateral, and posterolateral diaphysis, are multiple smaller shallow pits of varying shape. Numerous small striations, oriented perpendicular to the long axis of the shaft, are evident across the diaphysis, but are particularly prevalent on the anterior surface. The subtrochanteric mediolateral diameter measures 28.1 mm. The subtrochanteric anteroposterior diameter measures 20.8 mm. The linea aspera is palpable, but very weakly-developed. The pectineal line is almost undetectable, presenting as a smooth, small ridge descending from the inferior corner of the lesser trochanter, flattening as it extends distally. The gluteal tuberosity is more pronounced, posteriorly positioned, and forms a slight third trochanter proximally. The diaphysis is irregularly fractured (~80 mm distal to the inferior border of the lesser trochanter) such that the lateral aspect of the shaft extends ~18 mm distal to the fracture plane through the anterior, posterior, and medial diaphysis. The edges of the broken diaphysis are jagged and lighter in color than the surrounding bone, consistent with postdepositional or postmortem fractures. The anterior surface of the distal diaphysis, abutting the fracture, shows cortical bone flaking.

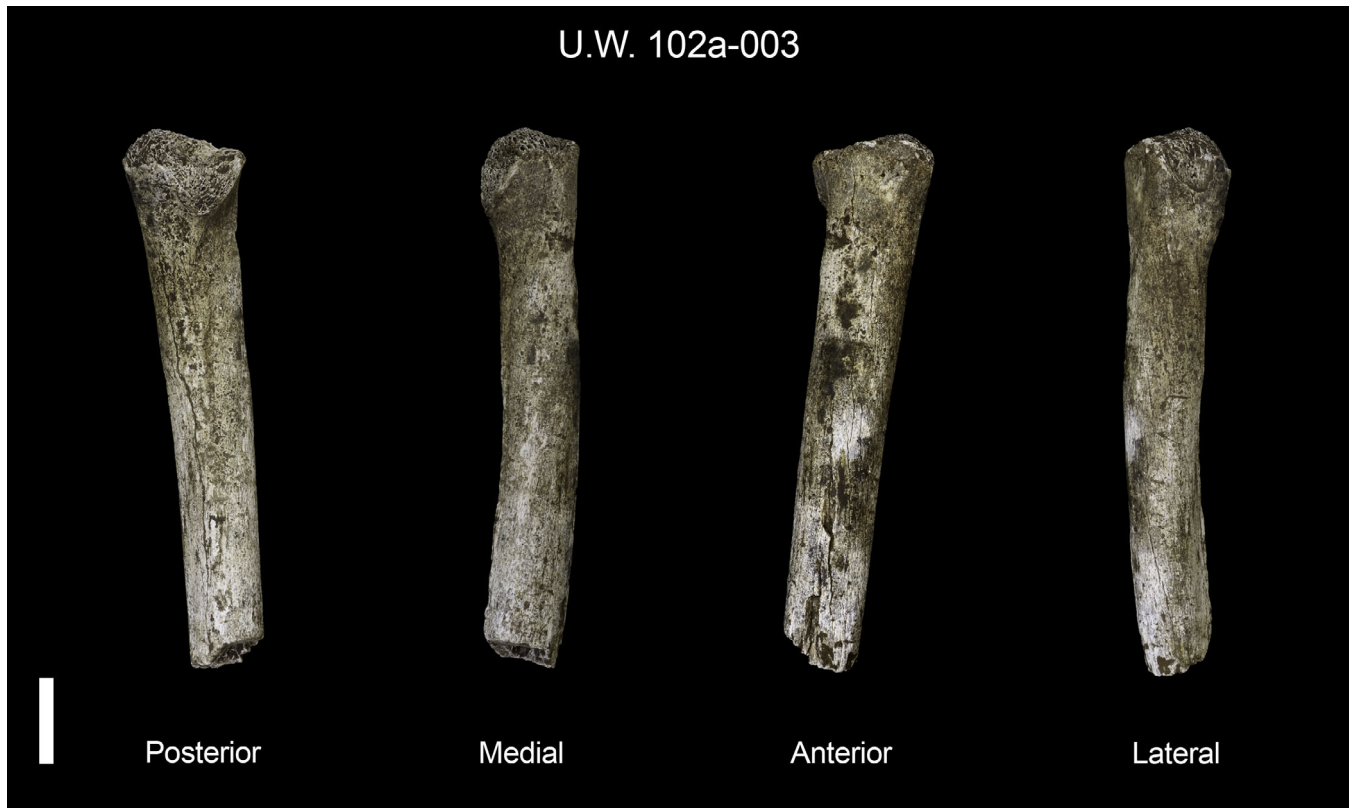


**FIGURE 6** Partial left proximal femur U.W. 102a-003. Scale bar = 2.5 cm

Cortical thickness at the distal break is 7.8 mm medially, 7.4 mm laterally, 7.3 mm posteriorly, and 7.3 mm anteriorly (thickest posteromedially = 8.9 mm). External diaphyseal dimensions just proximal to the shaft break are 23.2 mm ML by 20.7 mm AP. Superficially, the anterior surface of the diaphysis is, overall, smoother than the posterior surface. The color of the specimen ranges from very light brown to dark brown, with small and patchy iron oxide (red) and manganese oxyhydroxide (black) stains present throughout.

U.W. 102a-003 (Figure 6) and U.W. 102a-004 (Figure 7) are two left femoral elements preserving 148.7 mm SI from the level of the lesser trochanter to near midshaft (U.W. 102a-003) and 182.5 mm SI from near midshaft to the distal extent of the intercondylar fossa (U.W. 102a-004). The two elements conjoin at the lateral diaphysis (Hawks et al., 2017), but there are notable differences in patina, edge wear, and breakage patterns between the distal end of U.W. 102a-003 and the proximal end of U.W. 102a-004 and the elements have no points of contact posteriorly, medially, or anteriorly.

The femoral head, neck, greater trochanter, and associated structures of U.W. 102a-003 are missing due to an oblique fracture through the lesser trochanter that extends proximolaterally to the most proximal diaphysis, exposing underlying trabecular bone. The subtrochanteric diaphyseal dimensions are 25.2 mm ML by 20.9 mm AP. The gluteal line is indistinct. The pectineal line and linea aspera are rugose. While the linea aspera does form a small crest, there is only a very weak pilaster. Slight sagittal plane curvature (anteroposterior bowing) of the diaphysis is evident in the medial and lateral views.

Numerous longitudinally-oriented cracks, consistent with postmortem drying, are present on all aspects of the diaphysis, but are most prominent on the anterior surface and penetrate deepest at the distal end of the specimen. A particularly notable fissure on the posterior diaphysis runs adjacent to the linea aspera, extending from level of the inferior aspect of the lesser trochanter to the distal diaphyseal breakage. Short striations, oriented perpendicular to the long axis of the shaft, are concentrated on the lateral aspect of the diaphysis. The anterior aspect of the diaphysis exhibits multiple large, amorphous, black stains, consistent with manganese oxyhydroxide. The coloration of the distal end of the specimen is lighter (off white) than the rest of the specimen (light brown/brown). The diaphysis terminates at an oblique break, ~112 mm distal to the inferior border of the lesser trochanter. At the level of the break, the diaphysis is elliptical in cross-section, with the major axis of the ellipse running from anterolateral to posteromedial. The cortical bone at the distal break is thick, measuring 8.7 mm at its thickest portion (posteromedial), 7.5 mm medially, 7.5 mm laterally, 8.0 mm posteriorly, and 6.7 mm anteriorly (estimated due to superficial damage on the distal anterior shaft).

The proximal end of the U.W. 102a-004 diaphysis is jagged and deformed. Some of the broken edges show the white internal structure of the bone. Proximally, a sizeable, irregularly-shaped, fragment is missing from the lateral aspect of the diaphysis. Altogether, this pattern of damage and coloration is consistent with a post-depositional fracture. Numerous short, wide, transversely-oriented lacerations are present on the posterior aspect of the element. As on U.W. 102a-003,



there are numerous fine cracks, running longitudinally, primarily on the anterior, medial, and lateral diaphyseal surfaces. The continuation of the linea aspera from U.W. 102a-003 is visible to its distal extent. The lateral supracondylar line is palpable, but poorly developed, while the medial supracondylar line is barely detectable. Anteriorly, there is a very well-developed, concave suture hollow filled with several foramina. The patellar groove is smooth, convex SI, and concave ML. The lateral condyle is broken anteroposteriorly, through the lateral lip, and is largely missing, exposing a 38.2 mm AP by 33.3 mm SI section of trabecular bone. The medial condyle is broken obliquely, also exposing trabecular bone. Though the condyles are broken, remnants of the medial and lateral patellar lips are sufficient to show a markedly anterior projecting lateral lip (relative to both the medial lip and patellar groove). The partial intercondylar notch measures 16.3 mm ML and contains a well-developed pit posterolaterally for the anterior cruciate ligament.

Additional details about the preservation of U.W. 102a-001, -003, and -004, specifically, and the Lesedi fossil assemblage, generally, can be found in Hawks et al. (2017; pp. 30–32, 40–42, and supplementary file 5).

### 3.2 | Reconstructions and measurement estimations

Estimates of FHD and NB, derived from reconstructions of the damaged U.W. 102a-001 femoral head and anterior neck, are 36.0 mm and 17.5 mm, respectively.

Overall, the results of our error analyses indicate that our sphere-fitting method produces reasonably accurate estimates of empirical FHD in modern humans and fossil hominins (Figure 8, Tables 2 and 3). The regression slopes less than 1.0 indicate that the sphere-fitted diameters tend to slightly exceed true FHD (e.g., estimates falling to the right of the dashed isometry lines in Figure 8). Interestingly, many fossil hominins, especially at larger sizes, appear to have larger FHDs than predicted for *H. sapiens* of the same sphere size, possibly

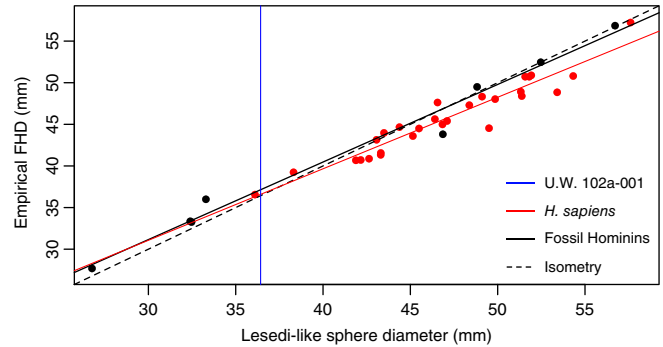


**FIGURE 8** Empirical superoinferior head diameter (FHD; mm) plotted against fitted sphere (estimated) diameter (mm) in *H. sapiens* and fossil hominins. The solid lines depict least squares regressions. The dashed line represents isometry ( $y = x$  or estimated = empirical). Red dots and lines represent *H. sapiens*. Black dots and lines represent fossil hominins. The vertical blue line represents the average sphere-fit diameter for U.W. 102a-001

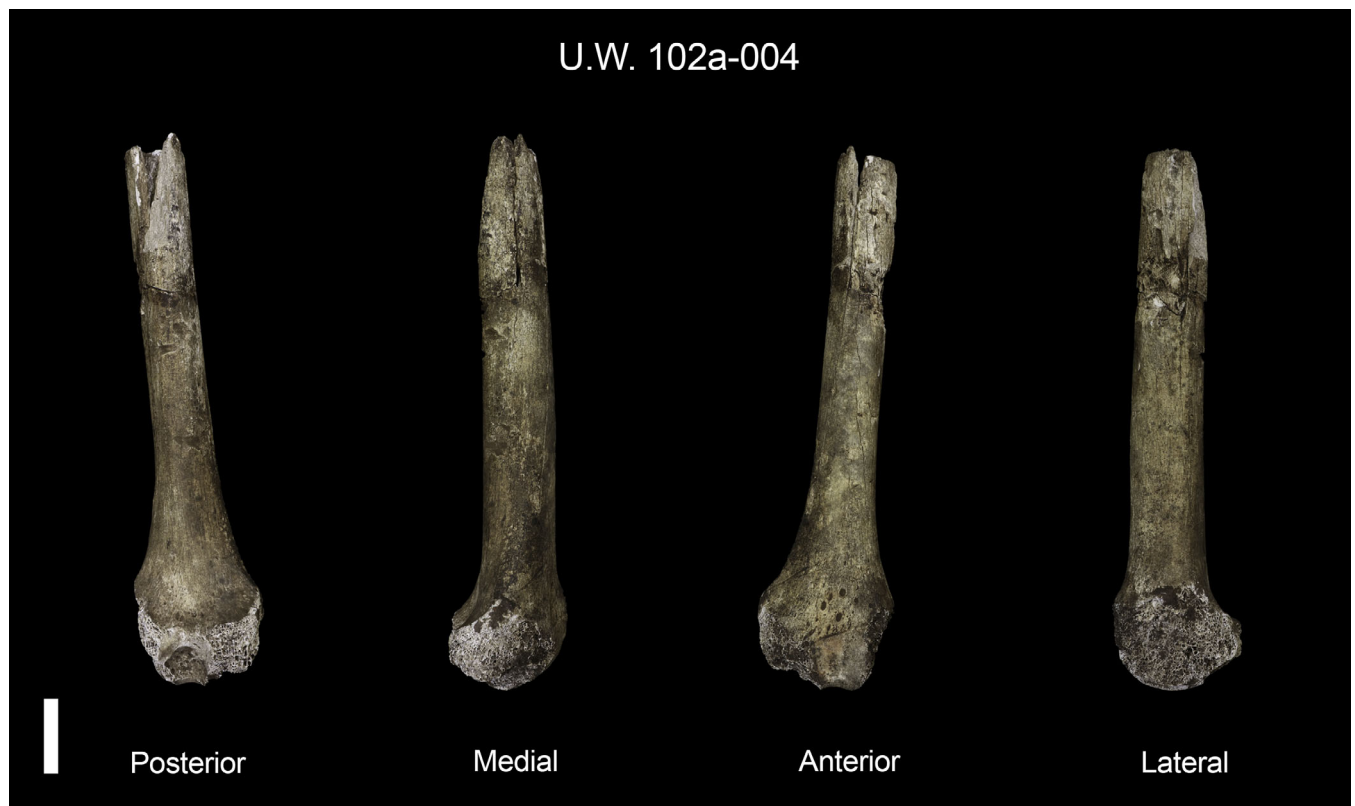


**FIGURE 7** Partial left distal femur U.W. 102a-004. Scale bar = 2.5 cm

TABLE 4 Comparative proximal femur metrics

Specimen/species/ group	Head SI (mm)	Neck SI (mm)	Neck AP (mm)	Neck shape (AP/SI) × 100	Neck-shaft angle (degrees)	Neck length <sup>a</sup> (mm)	Subtroch. AP (mm)	Subtroch. ML (mm)	Platymetric index	Neck length/ subtrochanteric dimensions <sup>b</sup>
U.W. 102a-001	36.0 <sup>c</sup>	24.4	17.5 <sup>c</sup>	71.7	120.0	33.9	20.8	28.1	74.0	1.40
U.W. 102a-003	-	-	-	-	-	-	20.9	25.2	82.9	-
<i>Homo naledi</i> (Dinaledi) <sup>d</sup>	35.5 ± 0.4 35.2–35.8 (n = 2)	23.3 ± 1.8 21.7–25.8 (n = 4)	16.4 ± 1.1 15.0–17.5 (n = 4)	70.7 ± 7.0 65.5–80.6 (n = 4)	117.3 ± 1.4 115.7–118.2 (n = 3)	31.1 ± 3.1 27.4–34.3 (n = 4)	18.8 ± 1.8 15.4–21.6 (n = 11)	25.0 ± 3.7 19.1–31.4 (n = 11)	75.7 ± 6.8 64.8–87.1 (n = 11)	1.4 ± 0.2 1.3–1.6 (n = 3)
<i>Gorilla gorilla</i>	45.5 ± 5.6 36.5–54.7 (n = 47)	31.3 ± 4.0 24.2–39.1 (n = 47)	25.5 ± 3.7 17.1–33.0 (n = 47)	81.3 ± 4.7 70.6–92.6 (n = 47)	119.0 ± 4.3 111.6–127.3 (n = 20)	32 ± 6.2 21.6–48.9 (n = 47)	31.9 ± 4.0 24.7–39.3 (n = 47)	38.3 ± 4.8 29.3–45.9 (n = 47)	83.2 ± 4.0 76.5–93.8 (n = 47)	0.9 ± 0.2 0.5–1.4 (n = 47)
<i>Pan troglodytes</i>	33.5 ± 2.1 23.7–37.4 (n = 42)	23.4 ± 1.9 19.7–27.6 (n = 42)	20.0 ± 1.3 17.9–22.8 (n = 42)	85.9 ± 5.1 76.7–95.7 (n = 42)	124.1 ± 4.6 115.0–130.9 (n = 20)	27.3 ± 4.3 20.2–40 (n = 42)	23.4 ± 1.4 20.6–26.2 (n = 42)	27.7 ± 1.9 23.7–32.4 (n = 42)	85.0 ± 5.5 71.1–95.5 (n = 42)	1.1 ± 0.2 0.8–1.8 (n = 42)
<i>Homo sapiens</i>	43.0 ± 4.3 32.1–52.4 (n = 195)	31.5 ± 3.6 23.7–40.8 (n = 170)	25.9 ± 3.4 17.2–34.0 (n = 170)	82.4 ± 5.9 63.9–104.3 (n = 170)	124.4 ± 3.8 114.0–132.0 (n = 100)	33.4 ± 4.0 23.5–42.8 (n = 83)	25.7 ± 2.6 19.7–32.8 (n = 195)	31.9 ± 3 23.4–39.3 (n = 195)	80.8 ± 6.8 56.1–96.6 (n = 195)	1.2 ± 0.1 0.9–1.5 (n = 83)
<i>Australopithecus afarensis</i> <sup>e</sup>	35.9 ± 4.9 28.6–40.2 (n = 5)	25.1 ± 3.3 21.4–29.8 (n = 5)	19.5 ± 3.3 15.7–24.9 (n = 6)	78.8 ± 3.9 73.4–83.6 (n = 5)	121.8 ± 3.6 117.0–125.0 (n = 5)	30.6 ± 10.0 23.5–37.7 (n = 2)	23.0 ± 5.1 16.9–30.6 (n = 11)	30.2 ± 5.2 23.5–38.9 (n = 11)	75.8 ± 5.9 66.4–88.4 (n = 11)	1.1 ± 0.0 1.1–1.1 (n = 2)
<i>Australopithecus africanus</i> <sup>f</sup>	33.1 ± 2.7 29.1–37.6 (n = 18)	23.8 ± 2.5 20.1–27.3 (n = 11)	17.0 ± 2.3 13.4–21.3 (n = 9)	70.3 ± 7.0 59.8–78.0 (n = 9)	120.7 ± 3.1 118.0–124.0 (n = 3)	32.2 ± 14.1 22.2–42.1 (n = 2)	18.1 (n = 1)	22.4 (n = 1)	80.8 (n = 1)	-
Robust <i>Australopithecus</i> ( <i>Paranthropus</i> ) <sup>g</sup>	33.9 ± 3.9 28.6–41.3 (n = 12)	25.6 ± 3.9 19.1–33.0 (n = 10)	17.1 ± 1.5 15.0–19.5 (n = 10)	67.7 ± 8.1 55.5–83.8 (n = 10)	116.8 ± 2.8 114.0–120.0 (n = 4)	36.6 ± 5.0 31.2–43.1 (n = 4)	23.6 ± 1.4 22.4–26.0 (n = 6)	30.7 ± 2.4 26.3–33.0 (n = 6)	77.2 ± 5.4 71.5–85.2 (n = 6)	1.3 ± 0.2 1.1–1.6 (n = 4)
<i>Australopithecus sediba</i> <sup>h</sup>	32.9 ± 0.2 32.7–33.0 (n = 2)	22.9 ± 0.6 22.4–23.3 (n = 2)	16.9 ± 0.4 16.6–17.1 (n = 2)	73.8 ± 0.5 73.4–74.1 (n = 2)	112.5 (n = 1)	28.9 (n = 1)	20.3 (n = 1)	26.4 (n = 1)	76.9 (n = 1)	1.3 (n = 1)
Early Pleistocene African/Georgian Homo <sup>i</sup>	40.9 ± 4.5 32.6–46.0 (n = 9)	28.2 ± 2.8 24–32.1 (n = 7)	21.2 ± 3.7 13.2–25.5 (n = 8)	79.8 ± 5.8 68.3–85.9 (n = 7)	119.3 ± 8.1 110.0–125.0 (n = 3)	38.0 ± 5.9 32.8–46.3 (n = 4)	24.4 ± 3.4 17.4–30.0 (n = 14)	33.1 ± 6.5 20.1–40.0 (n = 14)	75.1 ± 9.1 62.3–96.5 (n = 14)	1.4 ± 0.3 1.2–1.6 (n = 4)

(Continues)

**TABLE 4** (Continued)

Specimen/species/ group	Head SI (mm)	Neck SI (mm)	Neck AP (mm)	Neck shape (AP/SI) × 100	Neck-shaft angle (degrees)	Neck length <sup>a</sup> (mm)	Subtroch. AP (mm)	Subtroch. ML (mm)	Platymeric index	Neck length/ subtrochanteric dimensions <sup>b</sup>
Middle and Late Pleistocene African Homo <sup>c</sup>	50.4 ± 7.9 44.8–56.0 (n = 2)	41.4 (n = 1)	39.3 (n = 1)	84.6 ± 8.9 79.0–94.9 (n = 3)	135.0 (n = 1)	38.8 ± 2.3 37.2–40.4 (n = 2)	32.4 ± 3.4 30–34.8 (n = 2)	40.8 ± 0.07 40.7–40.8 (n = 2)	79.5 ± 8.5 73.5–85.5 (n = 2)	1.1 ± 0.1 1.0–1.2 (n = 2)

Linear measurements are in mm, areas in mm<sup>2</sup>, angular measurements are in degrees. Measurements are represented by mean ± SD, range, and sample size.

<sup>a</sup>Neck length from intertrochanteric crest to the lateral edge of the head.

<sup>b</sup>Neck length standardized by the subtrochanteric dimensions  $\sqrt{(\text{AP} \times \text{ML})}$ .

<sup>c</sup>Estimate. See Section 3.2.

<sup>d</sup>U.W. 101-002, U.W. 101-018, U.W. 101-271, U.W. 101-398, U.W. 101-421, U.W. 101-1136, U.W. 101-1300, U.W. 101-1391, U.W. 101-1434, U.W. 101-1475, U.W. 101-1482.

<sup>e</sup>A.L. 128-1, A.L. 152-2, A.L. 211-1, A.L. 288-1, A.L. 333-131, A.L. 333-142, A.L. 333-3, A.L. 333-95, A.L. 333w-40, A.L. 827-1, KSD-VP-1/1, MAK-VP-1/1.

<sup>f</sup>MLD 17, MLD 25, MLD 46, Sts 14, StW 179, StW 25, StW 300, StW 31, StW 311, StW 99, StW 361, StW 403, StW 443, StW 479, StW 501, StW 522, StW 527, StW 598.

<sup>g</sup>SK 14024, SK 3121, SK 3155B, SK 50, SK 82, SK 97, SKT1/LB-2, SKW 19, SKX 3121, TM 1605, OH 20, OH 80-12, KNM-ER 1500d, KNM-ER 1503, KNM-ER 1505.

<sup>h</sup>U.W.88-51 (MH2), U.W. 88-45,39 (MH1).

<sup>i</sup>BOU-VP-1/75, BOU-VP-1/9/63, BSN49/P2, D4167, D3901, KNM-WT 15000, KNM-ER 736, KNM-ER 737, KNM-ER 803A, KNM-ER 1472, KNM-ER 1475, KNM-ER 1481, KNM-ER 1808, KNM-ER 3228, KNM-ER 5880A, KNM-ER 5881, OH 28, OH 34, OH 62.

<sup>j</sup>Berg Aukas, KNM-ER 999, Kabwe E689 and E907.

indicating differences in femoral head shape (i.e., sphericity), between these groups. Regardless, both *H. sapiens* and fossil hominin regression lines cross or exceed the isometry line at the sphere size predicted for U.W. 102a-001, implying that its estimated FHD of 36.0 mm may even be a slight underestimate.

Mean percent prediction error is low in both fossil hominin (2.8%) and *H. sapiens* (3.4%) groups (Table 3). Moreover, 83% of all fitted spheres are within 5% of the empirical value. Contrastingly, the mean PPEs of spheres derived from small areas (single regions) of the acetabular lunate surface, analyzed in Hammond et al. (2013), are much higher, ranging between 32.3% and 64.3% within Hominidae (PPEs are within the lower end of this range when considering anthropoids more broadly). Thus, while a small area of the acetabular lunate surface is insufficient to accurately predict acetabular size, a small area of the posterior subchondral surface of the femur head does appear to be sufficient to accurately estimate FHD among hominins.

With respect to the femoral neck and our estimate of NB, given that our U.W. 102a-001 neck reconstruction utilized a largely qualitative methodology that cannot be uniformly applied to other hominin femoral neck reconstructions, error could not be assessed. Accordingly, the accuracy of our NB estimation is unknown, however, when the typical shape of the *H. naledi* femoral neck is considered, we believe it likely that the U.W. 102a-001 NB estimate presented here represents the maximum reasonable value for this measure. All Dinaledi femora exhibit a flattened anterior border at and near mid-neck. As reconstructed, the anterior border of U.W. 102a-001 is gently convex, exhibiting a degree of curvature comparable to that of its posterior border and greater than that of the Dinaledi femora. A larger estimated AP diameter than that presented here would indicate an atypically shaped (for *H. naledi*) convex anterior border, that morphologically contrasts the shape observed in adjacent, preserved portions of the U.W. 102a-001 femoral neck. As such, while we cannot entirely dismiss the possibility of an anomalously convex anterior border of the U.W. 102a-001 mid-neck, we consider it improbable, and conservatively propose that the true neck breadth of the specimen is, most likely, between the estimated value of 17.5 mm and the preserved value of 16.1 mm (a known underestimate).

### 3.3 | Comparative anatomy

Overall, the three femoral elements from the Lesedi chamber are morphologically consistent with the femoral remains from the Dinaledi chamber (Berger et al., 2015; Marchi et al., 2017), and expand the range of variation observed in the Dinaledi sample. The neck dimensions, neck shape, neck length, subtrochanteric dimensions, platymeric index, and degree of femoral anteversion of U.W. 102a-001 and (for a subset of these measures) U.W. 102a-003 fall within the range of the Dinaledi femora, and commonly within one standard deviation of the Dinaledi mean, for each respective metric (Table 4; Figures 9–11). The neck-shaft angle of U.W. 102a-001 is 120°, placing it just under 2° greater than the Dinaledi maximum. The suite of Lesedi femur values is most consistent with the Dinaledi femora among comparative hominin femora.

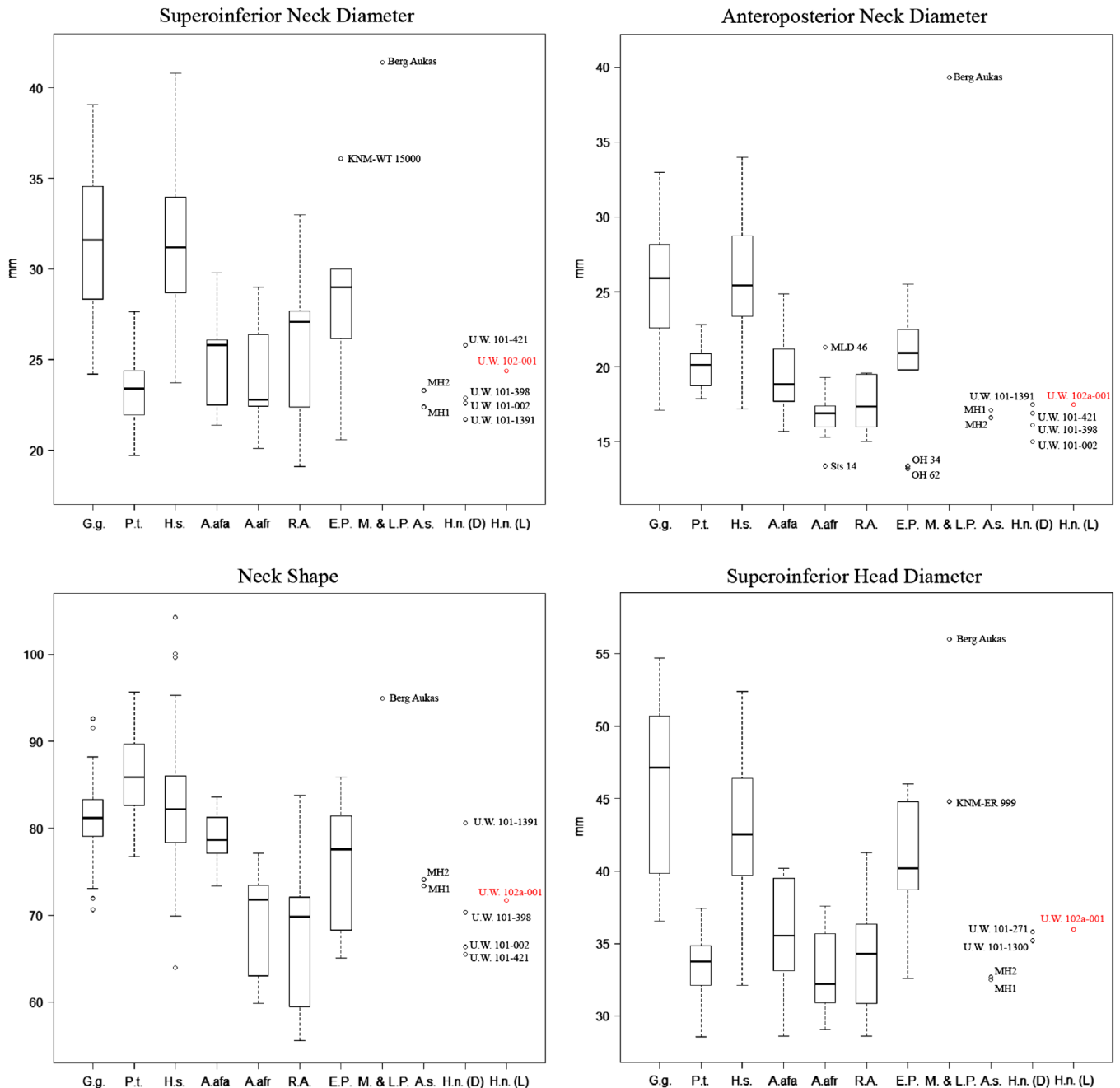


**FIGURE 9** Superoinferior neck diameter (NH), anteroposterior neck diameter (NB), neck shape (NB/NH  $\times$  100), and superoinferior head diameter (FHD) boxplots for extinct and extant hominid taxa. Boxes include 25–75% quartiles with a mean line; whiskers extend to maximum and minimum values  $<1.5$  times interquartile range. Key: G.g.—*Gorilla gorilla*, P.t.—*Pan troglodytes*, H.s.—*Homo sapiens*, A.afa.—*Australopithecus afarensis*, A.afr.—*Australopithecus africanus*, R.A.—*Robust Australopithecus (Paranthropus)*, A.s.—*Australopithecus sediba*, E.P.—*Early Pleistocene African/Georgian Homo*, M. & L.P.—*Middle and Late Pleistocene African Homo*, H.n. (D)—*Homo naledi (Dinaledi)*, H.n. (L)—*H. naledi (Lesedi)*

DFA plots U.W. 102a-001 within the bounds of the convex hull formed by *H. naledi* specimens from Dinaledi (Figure 12). The highest posterior probability for group membership for U.W. 102a-001 is *H. naledi* [ $P(G = g|D = d) = 0.407$ ]; the second highest group posterior probability is *Australopithecus* [ $P(G = g|D = d) = 0.304$ ] (Table S1). Though 81% of *H. sapiens* are correctly classified, only 42.9% of australopiths and none of the four fossil *Homo* specimens are correctly classified (Table 5). Overall, 69.4% of cross-validated grouped cases are correctly

classified. U.W. 102a-001 is differentiated from *H. sapiens* along Function 1 and is intermediate to fossil *Homo* and *Australopithecus* along Function 2. All fossil hominin specimens in the DFA are largely separated from *H. sapiens* along Function 1, which accounts for 81.9% of the variance. Anteroposterior neck breadth and neck length are the primary driving factors, with specimens possessing longer and AP compressed necks located on the right. Fossil hominin groups are differentiated from each other along Function 2, accounting for 16.6% of the variance.

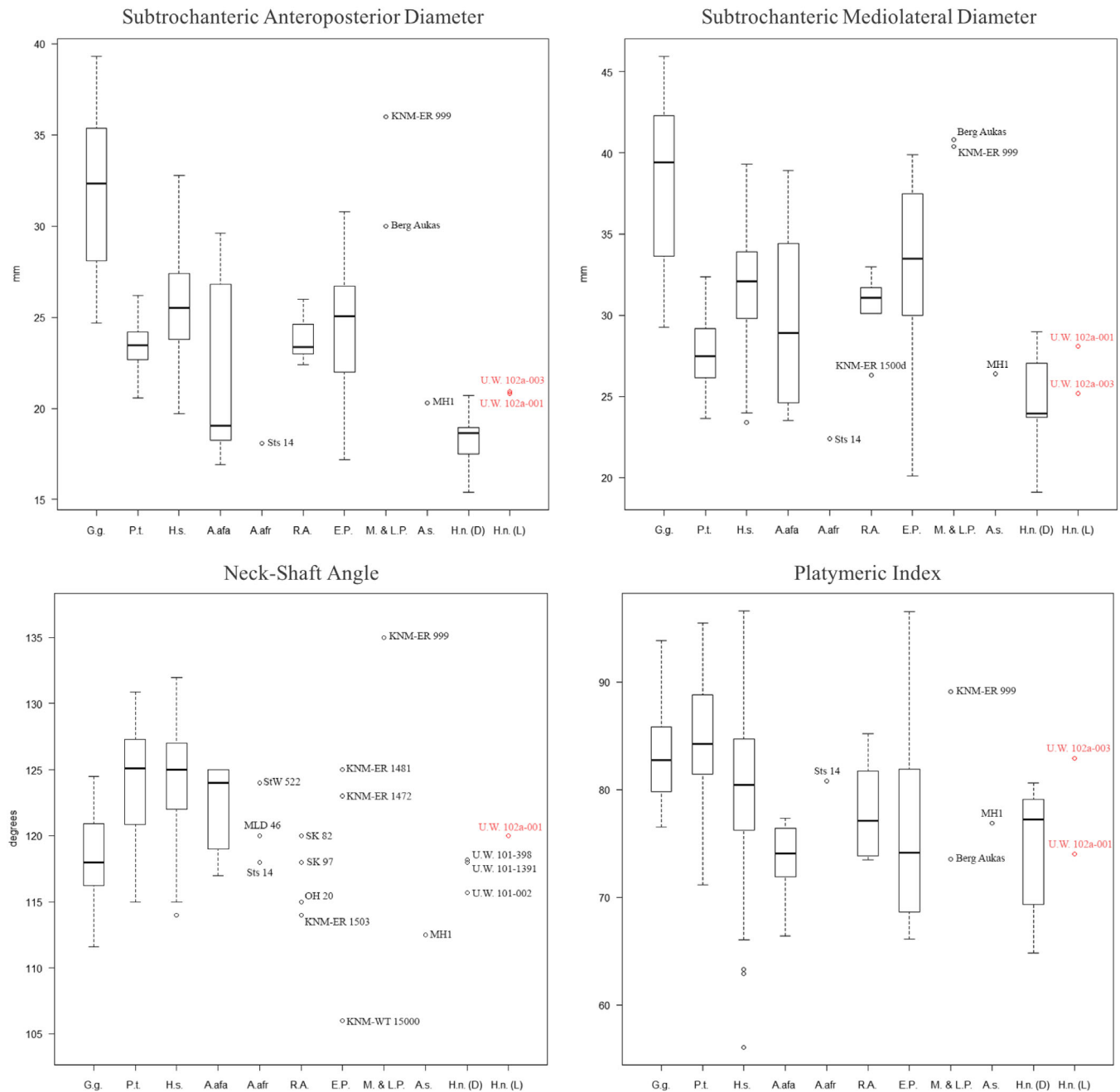


**FIGURE 10** Subtrochanteric anteroposterior diameter (SAP), subtrochanteric mediolateral diameter (SML), neck-shaft angle (NSA), and platymetric index (SAP/SML  $\times$  100) boxplots for extinct and extant hominid taxa. Boxes include 25–75% quartiles with a mean line; whiskers extend to maximum and minimum values  $<1.5$  times interquartile range. Key: G.g.—*Gorilla gorilla*, P.t.—*Pan troglodytes*, H.s.—*Homo sapiens*, A.afa.—*Australopithecus afarensis*, A.afr.—*Australopithecus africanus*, R.A.—*Robust Australopithecus (Paranthropus)*, A.s.—*Australopithecus sediba*, E.P.—*Early Pleistocene African/Georgian Homo*, M. & L.P.—*Middle and Late Pleistocene African Homo*, H.n. (D)—*Homo naledi (Dinaledi)*, H.n. (L)—*H. naledi (Lesedi)*

Again, neck length factors prominently (in the positive direction) along with subtrochanteric anteroposterior diameter (in the negative direction). Notably, three of the *H. naledi* femora included in the DFA (U.W. 102a-001, U.W. 101-002, and U.W. 101-1391) are within the range of human variation. Moreover, though U.W. 102a-001 is within the boundaries of the *H. naledi* convex hull, it resides nearest SK 97 (*A. robustus*), along with Dinaledi specimen U.W. 101-002 and two modern humans.

The Lesedi femur U.W. 102a-001 differs from the Dinaledi femora with respect to some features of the neck. The most unique trait of the Dinaledi proximal femora is a mediolaterally expanded groove on the superior surface of the neck, possibly for the attachment of internal obturator and gemelli muscles, associated with two adjacent mediolaterally-oriented pillars (one positioned superoanteriorly and one positioned inferoposteriorly; Marchi et al., 2017). Damage to the region of the neck that would bear the superoanterior pillar prevents

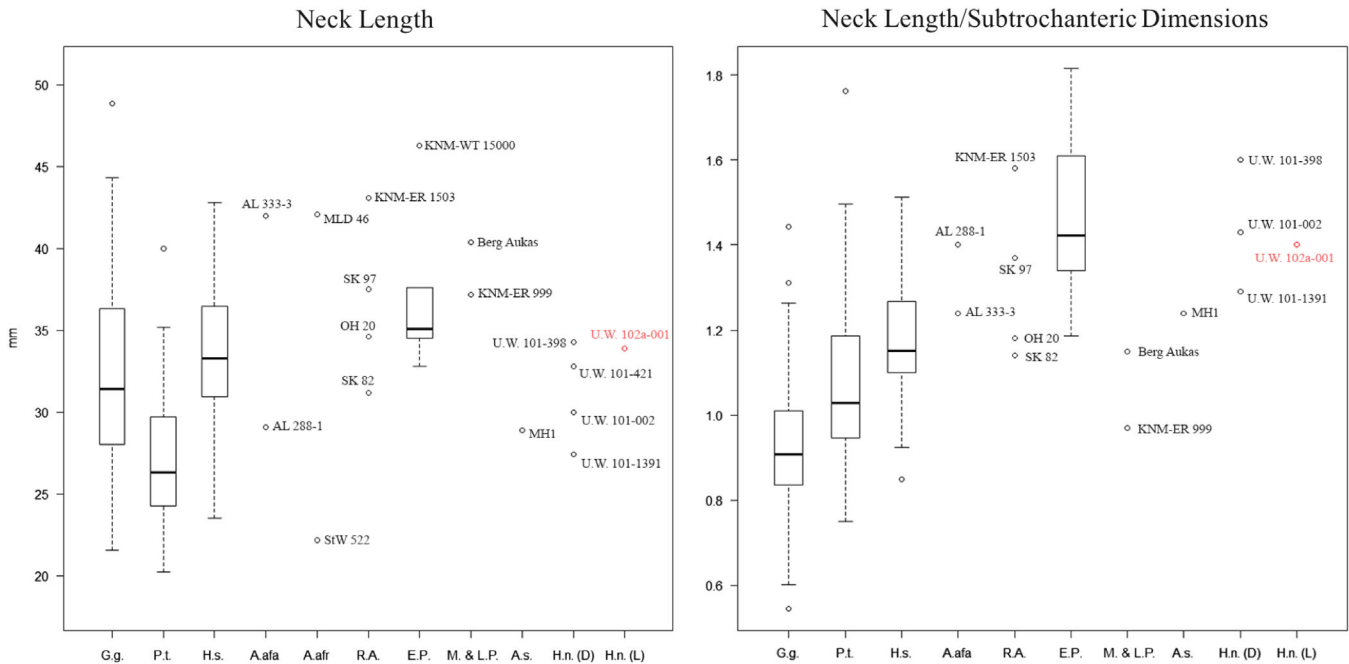


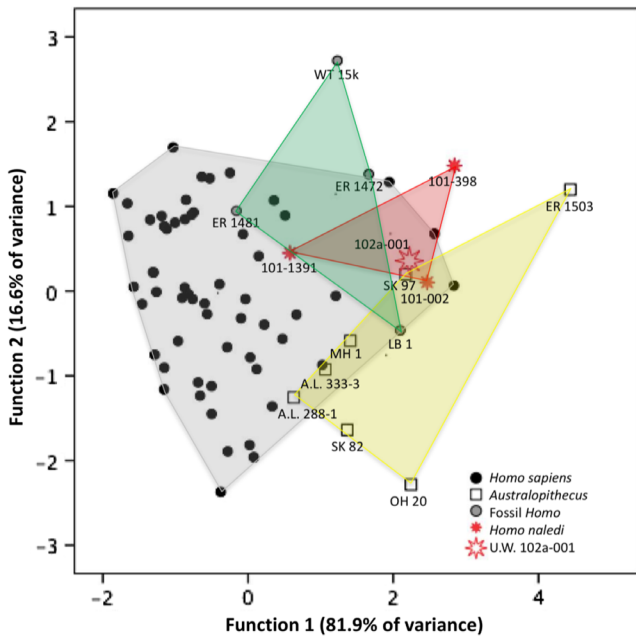
**FIGURE 11** Neck length (NL) and neck length/subtrochanteric dimensions (NL/ $\sqrt{[SAP \times SML]}$ ) boxplots for extinct and extant hominid taxa. Boxes include 25–75% quartiles with a mean line; whiskers extend to maximum and minimum values  $<1.5$  times interquartile range. Key: G.g.—*Gorilla gorilla*, P.t.—*Pan troglodytes*, H.s.—*Homo sapiens*, A.afa.—*Australopithecus afarensis*, A.afr.—*Australopithecus africanus*, R.A.—*Robust Australopithecus (Paranthropus)*, A.s.—*Australopithecus sediba*, E.P.—*Early Pleistocene African/Georgian Homo*, M. & L.P.—*Middle and Late Pleistocene African Homo*, H.n. (D)—*Homo naledi (Dinaledi)*, H.n. (L)—*H. naledi (Lesedi)*

evaluation of this structure on U.W. 102a-001. An inferoposteriorly positioned pillar, however, is preserved on U.W. 102a-001. (Figures 13 and S2). Though the pervasive damage abutting the pillar precludes an unequivocal assessment of pillar expression, compared to the Dinaledi femora, the U.W. 102a-001 inferoposterior pillar appears less defined. U.W. 102a-001 also differs from the Dinaledi femora (and a variety of other hominin taxa) by the concavity of its posterior surface and the squareness/flatness of its inferior surface, particularly at and near the neck-shaft junction (Figure 14). Some degree of posterior neck concavity is present in the Dinaledi femora (especially U.W. 101-002 and U.W. 101-398), but this concavity is much more pronounced in U.W. 102a-001. Similarly, other hominin femora (including StW 99, A.L. 333-3, and A.L. 333-95) have flattened inferior femoral necks near the neck-shaft junction, but none are as expanded as that of U.W. 102a-001. The Dinaledi femora have largely narrow, rounded, convex inferior necks, though U.W. 101-398 does exhibit some degree of flattening. The significance of this femoral neck morphological variation between U.W. 102a-001 and the Dinaledi femora, however, is presently unknown. Accordingly, while we highlight these traits, further work is necessary to determine if any of the noted variation is functionally and/or evolutionary meaningful.

Some features not entirely preserved in the Dinaledi femora are more clearly evident in the Lesedi femoral sample. Chief among these are the anteriorly projecting lateral lip and sutured hollow of U.W. 102a-004 distal femur (Figure S3). Both features were suspected to be present in the Dinaledi femora, but no distal femoral fragment in the Dinaledi assemblage was complete enough to unambiguously

confirm the existence of a sutured hollow or degree of lateral lip projection (Marchi et al., 2017). U.W. 102a-004 preserves much more of the lateral lip than the Dinaledi archetype for the feature, immature specimen U.W. 101-1120, substantiating the evidence for an anteriorly projecting lateral lip in *H. naledi* (Marchi et al., 2017). Lateral lip projection, functionally helping to prevent dislocation of the patella during bipedal locomotion, is present in both *Australopithecus* and *Homo* femora, but with varying degrees of prominence (Aiello & Dean, 1990; Clark, 1947; DeSilva et al., 2013; Heiple & Lovejoy, 1971). Due to damage on the condyles of U.W. 102a-004, lateral lip projection can only be assessed qualitatively, and appears less pronounced than in *A. sediba*, comparable to *H. sapiens*, and more pronounced than most specimens of *A. afarensis* and *A. africanus* (including TM 1513, A.L. 334-4, and A.L. 129-1) and some specimens attributed to *Homo* (like KNM-ER 1472). Additionally, the patellar surface in U.W. 102a-004 is anteriorly expanded, a feature that could not be evaluated in U.W. 101-1120 and may be related to the prominent lateral lip (Lovejoy, 2007).

No femur in the Dinaledi assemblage is as complete as the U.W. 102a-003/U.W. 102a-004 rejoined left femur, allowing for improved estimations of total length and evaluation of midshaft dimensions. Hawks et al. (2017) estimated the total length of the femur to be 375 mm. If this value is accurate, the dimensions of the diaphysis at midshaft are  $\sim 23$  mm AP by 21 mm ML; accordingly, the femur is marked by an AP expanded diaphysis at midshaft (pilasteric index = 1.09). Notably, even if the total length of the composite femur is estimated incorrectly, the Lesedi femur is still almost certainly marked by an AP expanded diaphysis at midshaft, as the AP dimensions of the diaphysis



Variable	Function 1	Function 2	Function 3	Wilks' Lambda	Signif. (P)
Neck AP	-.946	.103	.134	.839	.007
Neck Length	.774	.608	.012	.590	.000
Neck SI	-.487	-.199	.383	.657	.000
Subtroch. AP	.038	-.639	.410	.937	.215
Subtroch. ML	.288	-.332	-.826	.916	.112

**FIGURE 12** Discriminant function analysis of the hominin proximal femur. The associated table lists incorporated measurements, structure matrix, and Wilks' lambda and significance values. Groups: *H. sapiens* (solid black circles; gray convex hull), *Australopithecus* (squares; yellow convex hull), Fossil *Homo* (gray circles; green convex hull), *H. naledi* from Dinaledi (small solid red stars; red convex hull). Lesedi femur specimen U.W. 102a-001 (large unfilled red star) falls within the boundaries of the Dinaledi and *H. sapiens* convex hulls

**TABLE 5** Discriminant function analysis cross-validation results

	<i>Homo sapiens</i>	<i>Australopithecus</i>	Fossil <i>Homo</i>	<i>Homo naledi</i>
<i>H. sapiens</i>	81%	5.2%	5.2%	8.6%
<i>Australopithecus</i>	28.6%	42.9%	0%	28.6%
Fossil <i>Homo</i>	25%	25%	0%	50%
<i>H. naledi</i>	0%	33.3%	66.7%	0%

exceed ML dimensions for much of the shaft. This differentiates *H. naledi* from most early Pleistocene *Homo* femora, which possess ML expanded midshafts, and aligns U.W. 102a-003/–004 with a minority of fossil *Homo* femora, including KNM-ER 5881 (which, coincidentally, has identical midshaft proportions to U.W. 102a-003/004), D3160, D4167, and OH 62, each of which have pilasteric indices (midshaft AP/ML) greater than 1 (Ruff, 1995; Ward et al., 2015).

### 3.4 | Bilateral asymmetry

Our evaluation of the morphological variation between U.W. 102a-001 and U.W. 102a-003 supports the hypothesis that these bones

may come from two different individuals. First, the entheses of U.W. 102a-001 are considerably less developed than those of U.W. 102a-003. This includes a reduced linea aspera and pectineal line in U.W. 102a-001 (right) compared to U.W. 102a-003 (left). Second, though the lesser trochanters of both specimens are damaged, the remnants reveal a contrasting morphology between U.W. 102a-001 and -003, particularly with respect to the angle formed at the medial borders (Hawks et al., 2017). Third, while the anteroposterior subtrochanteric dimensions of the two proximal femora are comparable (0.5% difference), the mediolateral diameter of U.W. 102a-001 (28.1 mm) is 10.9% larger than the same dimension in U.W. 102a-003 (25.2 mm). Relative to a sample of 51 modern human femora, the Lesedi pairing is exceedingly asymmetrical with respect to ML diameter. Only a single human included in the study exhibits greater subtrochanteric diaphyseal asymmetry (12.6%) than the two Lesedi proximal femora, and this variation is between AP measures. The maximum human ML asymmetry in the sample is 7.3%. Results of exact randomization sampling reveal that Lesedi femora ML variation falls at the 72nd percentile (where a lower percentile corresponds to a higher sampling probability) of all sampled *H. sapiens* pairings (Figure S4;  $n = 2,601$ ). Accordingly, even in a moderate-sized sample of mixed-sex humans, the probability of pairing two femora as different as U.W. 102a-001 and -003 is fairly low. Importantly, the *H. sapiens* test sample did not include any individuals with obvious abnormalities, so these results cannot evaluate the likelihood of marked bilateral asymmetry in an individual with pathologies that may affect subtrochanteric dimensions (i.e., by influencing gait). That caveat aside, it appears unlikely (though not impossible) that U.W. 102a-001 and U.W. 102a-003 (along with the associated U.W. 102a-004) come from the same individual.

## 4 | DISCUSSION

The Dinaledi Chamber sample of *H. naledi* is impressively morphologically uniform (Berger et al., 2015; Garvin et al., 2017) and the Lesedi Chamber sample can mostly be encompassed within that low level of variability (Hawks et al., 2017). Nevertheless, the Lesedi femora do slightly expand the range of variation within *H. naledi*, particularly with respect to some qualitative features, including a potentially reduced inferoposterior neck pillar, a flattened inferior neck, and a weakly developed linea aspera in U.W. 102a-001. We hypothesize that these differences are consistent with normal variation within a slightly enlarged sample of *H. naledi*. Results of the DFA support this general assessment and, additionally, reflect the morphological affinities of the *H. naledi* proximal femora to those from other taxa. While the *H. naledi* femoral neck is relatively long, like early members of the genus *Homo*, absolute femoral neck length largely overlaps with members of *Australopithecus*. Ward et al. (2015) note a clear distinction between *Homo* and *Australopithecus* femoral neck shape indices (neck AP/SI diameter), with members of the latter genus exhibiting far greater AP compression (lower ratios) of the neck than members of the former. In their comparative fossil sample, D4167 (early *H. erectus* or *H. georgicus*) was the only

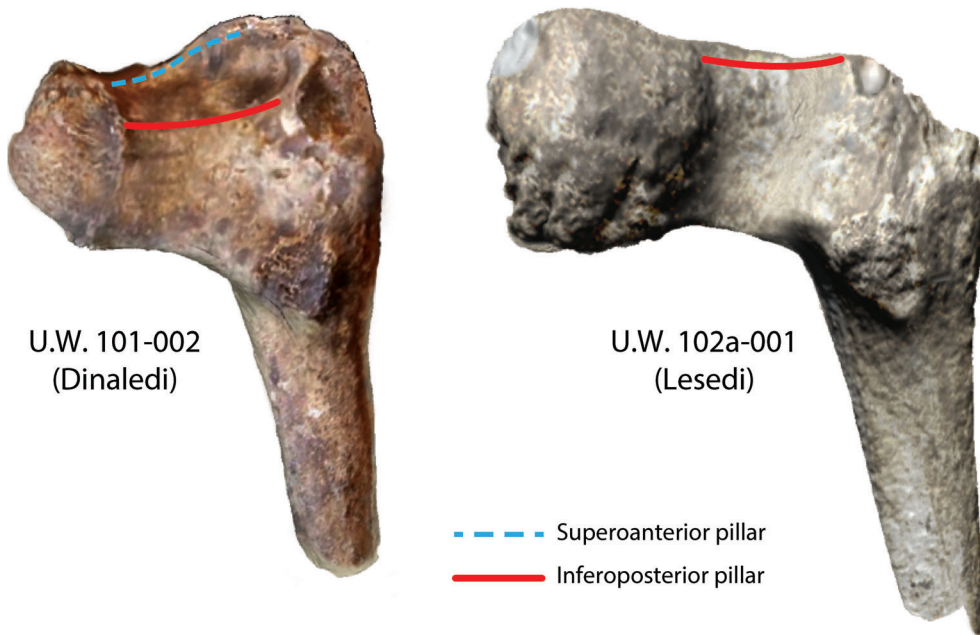


**FIGURE 13** Comparison of U.W. 101-002 (*H. naledi* from Dinaledi) and U.W. 102a-001 (*H. naledi* from Lesedi) superior neck pillars in an oblique superoposterior view. The dashed blue line corresponds to a superoanterior pillar. The solid red lines correspond to inferoposterior pillars. U.W. 102a-001 preserves an inferoposterior pillar, like all Dinaledi femora preserving the region, however, presence of a superoanterior pillar cannot be assessed due to breakage

*Homo* specimen to fall in the range of australopiths (Ward et al., 2015). Like D4167, all *H. naledi* femora found to date have decidedly australopith-like neck shape indices (Marchi et al., 2017). These primitive aspects of the proximal femur diverge from the morphological pattern observed on much of the rest of the *H. naledi* femur.

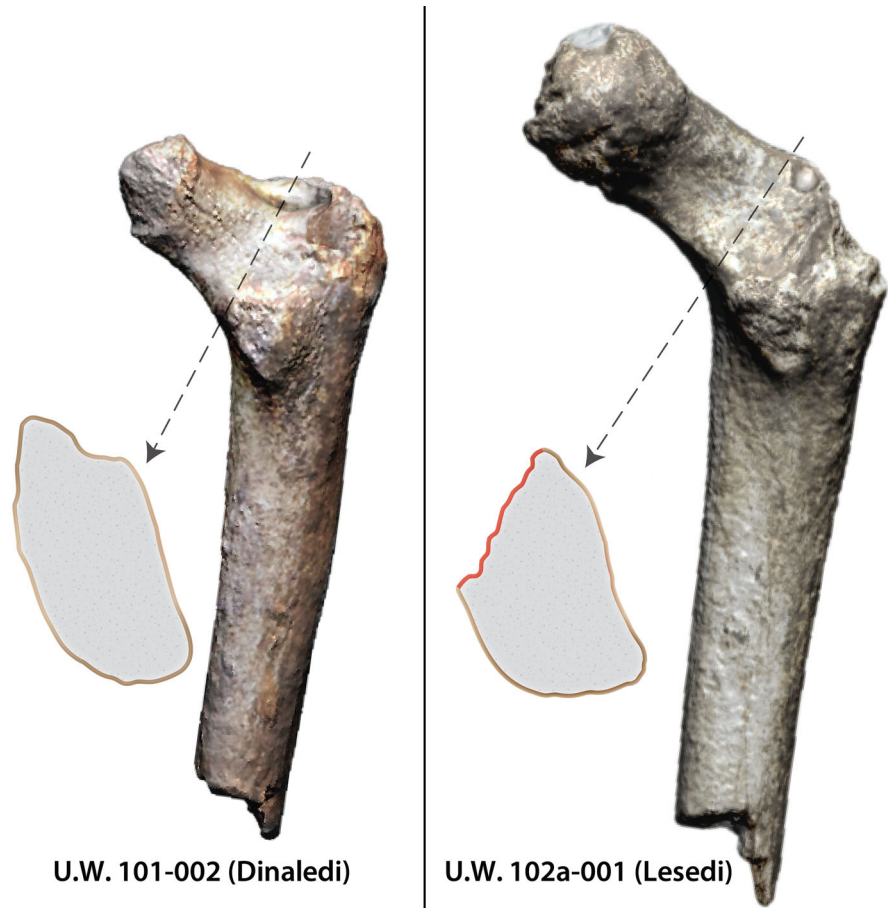
The femur is one of the most numerous postcranial elements recovered from the Dinaledi chamber, but no complete (or near complete) mature femora have, thus far, been identified from that locality. The distal femur is particularly poorly represented in the Dinaledi assemblage. U.W. 102a-004 is the most complete distal femur of *H. naledi* currently known, preserving a sustrochlear hollow and projecting lateral lip, previously speculated (Marchi et al., 2017), but now confirmed. Moreover, together U.W. 102a-003 and -004 represent the most complete mature femur of *H. naledi*, allowing for more accurate estimation of length (375 mm) and midshaft proportions (AP expanded). Each of these new findings carry some functional and/or taxonomic implications. The presence of a sustrochlear hollow has been taken as evidence of the capability of full knee extension (Tardieu, 2010). While this feature is evident in *A. sediba* and a number of fossils attributed to the genus *Homo* (see supplementary materials of Ward et al., 2015), the presence of a sustrochlear hollow and the capacity for full knee extension in *A. afarensis* is disputed (DeSilva et al., 2013; Tardieu, 2010). A distinct sustrochlear hollow on U.W. 102a-004 confirms the more preliminary identification of this feature on U.W. 101-545 and suggests that *H. naledi* was indeed capable of full knee extension. The presence of a distinct, anteriorly projecting lateral lip in *H. naledi* is not surprising given that this trait exists in most Plio-Pleistocene hominins (DeSilva et al., 2013; Heiple & Lovejoy, 1971; Lovejoy, 2007), but the prominence of the feature, comparable to *H. sapiens* and exceeded only by *A. sediba*, is notable. A prominent lateral lip serves to resist lateral dislocation of the patella during bipedal locomotion (related to a high femoral bicondylar angle and the action of *m. quadriceps femoris*; Heiple & Lovejoy, 1971).

The potentially associated (Lovejoy, 2007) anteriorly expanded patellar surface of U.W. 102a-004 is also important, because this feature is distinctive of the genus *Homo* and increases the mechanical advantage of *m. quadriceps femoris* (DeSilva et al., 2013; Lovejoy, 2007).

The finding of an AP expanded midshaft (pilasteric index = 1.09) in the conjoined U.W. 102a-003/-004 left femur is particularly notable. *H. naledi* femora are similar to many early *Homo* femora in having weak pilasters, thick cortices, and relatively long necks (Marchi et al., 2017; Ruff, 1995; Ward et al., 2015). *H. naledi*, however, appears to diverge from the typical early *Homo* midshaft shape pattern. Most early *Homo* femora and all African *H. erectus* femora are marked by ML expanded diaphyseal midshafts, while only a handful of Early Pleistocene *Homo* femora (namely, KNM-ER 5881 and OH 62 [early *Homo*, possibly *H. habilis*], D3160 and D4167 [early *H. erectus* or *H. georgicus*], and Trinil I [*H. erectus*; though the age of the fossil is uncertain (Bartsiokas & Day, 1993; Day & Molleson, 1973; Ruff, 1995)]) are like U.W. 102a-003/-004 in having AP expanded midshafts (Kennedy, 1983; Ruff, 1995; Ward et al., 2015). Ruff (1995) explained ML wide midshaft diaphyses as part of a suite of pelvic and femoral features, including a long femoral neck and wide biacetabular dimensions, that contribute to high ML bending moments in the proximal diaphysis. The lack of an ML expanded diaphysis in *H. naledi* and small-bodied early *Homo* specimens (e.g., OH 62, KNM-ER 5881, D3160, D416) and presence in larger early *Homo* specimens (e.g., KNM-ER 1481, KNM-ER 1472) supports this model, as body mass impacts bending moments of the femoral shaft. Ruff (1995) also linked the reduced expression of pilasters in early *Homo* to ML diaphyseal expansion. In the case of KNM-ER 5881 and OH 62, the reverse is indeed true, with their AP expanded midshafts accompanying pronounced pilasters (Ward et al., 2015). Partial support for the hypothesis that body size in early *Homo* impacts proximal femur morphology comes from the comparable (to *H. naledi*) suite of traits—including a



**FIGURE 14** Comparison of U.W. 101-002 (*H. naledi* from Dinaledi) and U.W. 102a-001 (*H. naledi* from Lesedi) transverse neck sections from the neck-shaft junction. 3D meshes of both specimens are shown in a posterior view. Transverse neck sections are gray with preserved periosteal borders colored light brown and damaged areas colored red. Note the more pronounced flattening of the inferior neck (transverse section bottom) and concavity of the posterior neck (transverse section right) in U.W. 102a-001 relative to U.W. 101-002



long femoral neck and AP expanded midshaft—found in the diminutive LB1 (*H. floresiensis*), though the LB1 pilasteric index is slightly lower (1.02) and it has no pilaster (Jungers et al., 2009).

The Dinaledi *H. naledi* assemblage was deposited between 335,000 and 236,000 years ago (Dirks et al., 2017). The Lesedi Chamber assemblage remains undated, but its morphological similarity to the Dinaledi sample may suggest it derives from a similar geological age (Hawks et al., 2017). This age does not impact the phylogenetic placement of *H. naledi*, but it may reveal a blind spot in previous comparisons of morphologically primitive species of *Homo*. While an AP expanded midshaft is somewhat surprising in a species with so many affinities to Early Pleistocene specimens attributed to *Homo*, the Dinaledi (and presumably Lesedi) remains are from the Middle Pleistocene. In this context, the *H. naledi* diaphyseal morphology is unremarkable, as most later *Homo* species, including *H. sapiens*, have high pilasteric indices (greater than 1; Aiello & Dean, 1990; Grine et al., 1995; Kennedy, 1984; Trinkaus & Ruff, 1999). Accordingly, proximate causes of shared diaphyseal midshaft morphology may differ between early (ca. 1.8–1.9 mya) femora, like KNM-ER 5881 and OH 62, and more recent ones, like those of *H. naledi*, *H. floresiensis* (Sutikna et al., 2016), and the Trinil femora (Kennedy, 1983; Ruff, Puymeryail, Macchiarelli, Sipla, & Ciochon, 2015).

Overall, the results presented here support the functional interpretation of the *H. naledi* lower limb as belonging to a species

adapted for long distance walking and, perhaps, running (Marchi et al., 2017). The significance of the unique femoral traits (e.g., superior neck pillars), however, remains unclear, as does the significance of any of the subtle morphological differences between otherwise metrically comparable Lesedi and Dinaledi femoral samples. While these features may be functionally relevant and differences between assemblages may be consistent with normal variation, future work is necessary to further investigate and specifically test these hypotheses.

#### ACKNOWLEDGMENTS

We thank the National Geographic Society and the National Research Foundation of South Africa for significantly funding the recovery and study of the remains from Rising Star. We are grateful to those who facilitated the collection of our comparative data: B. Billings, J. Chupasko, G. Grupe, Y. Haile-Selassie, K. Isler, L. Jellema, E. Langenegger, O. Lovejoy, E. Mbua, M. Morgan, D. Pilbeam, S. Potze, O. Röhrer-Ertl, E. Westwig, B. Zipfel. We thank K. Schroepfer and A. Harvey for assistance in the development and creation of figures. We appreciate I. Thompson and K. Walker for their aid in editing parts of the manuscript. We would also like to thank the University of the Witwatersrand and the Evolutionary Studies Institute for curating the material and hosting some authors and B. De Klerk for her help in coordinating visits.

## CONFLICT OF INTEREST

The authors have no competing interest to declare.

## AUTHOR CONTRIBUTIONS

C.S.W., M.G., S.E.C., and J.M.D. conceived the project. J.H. and L.R.B. administered the project. C.S.W., K.A.T., A.H.R., S.E.C., and J.M.D. described the fossils. C.S.W. made the figures. J.M.D. performed the discriminant function analysis. C.S.W., M.G., D.M., Z.D.C., A.P.V., and J.M.D. provided comparative data. All authors participated in the interpretation of results. C.S.W. wrote the article with contributions from all authors.

## DATA ACCESSIBILITY

Three-dimensional surface renderings of U.W. 102a-001 (<https://doi.org/10.17602/M2/M26233>), U.W. 102a-003, and U.W. 102a-004 (<https://doi.org/10.17602/M2/M26235>) are freely available for download from MorphoSource (<http://morphosource.org>; [Boyer, Gunnell, Kaufman, & McGeary, 2016]). The original fossils are available for study by researchers upon application to the Evolutionary Studies Institute at the University of the Witwatersrand, where they are curated.

## ORCID

Christopher S. Walker  <https://orcid.org/0000-0002-5173-2784>

John Hawks  <https://orcid.org/0000-0003-3187-3755>

Gabriel S. Yapuncich  <https://orcid.org/0000-0001-7371-5857>

Lee R. Berger  <https://orcid.org/0000-0002-0367-7629>

## REFERENCES

- 3D Systems. 2015. *Geomagic Design X [Computer software]*. Rock Hill, SC.
- Aiello, L. C., & Dean, C. (1990). *An introduction to human evolutionary anatomy*. New York, NY: Academic Press. <https://doi.org/10.1007/BF02547638>
- Bartsiokas, A., & Day, M. H. (1993). Electron probe energy dispersive X-ray microanalysis (EDXA) in the investigation of fossil bone: The case of Java man. *Proceedings of the Royal Society B: Biological Sciences*, 252, 115–123. <https://doi.org/10.1098/rspb.1993.0054>
- Berger, L. R., Hawks, J., de Ruiter, D. J., Churchill, S. E., Schmid, P., Delezene, L. K., ... Zipfel, B. (2015). *Homo naledi*, a new species of the genus homo from the Dinaledi chamber, South Africa. *eLife*, 4, e24232. <https://doi.org/10.7554/eLife.09560>
- Boyer, D. M., Gunnell, G. F., Kaufman, S., & McGeary, T. M. (2016). Morphosource: Archiving and sharing 3-D digital specimen data. *The Paleontological Society Papers*, 22, 157–181. <https://doi.org/10.1017/scs.2017.13>
- Clark, W. (1947). Observations on the anatomy of the fossil Australopithecinae. *Journal of Anatomy*, 81, 300–333. <https://doi.org/10.1002/ar.1091200107>
- Day, M., & Molleson, T. (1973). The trinit femora. In M. Day (Ed.), *Human evolution—Symposium of the Society for the Study of Human Biology* (Vol. 11, pp. 127–154). London: Taylor and Francis. <https://doi.org/10.1016/j.jhevol.2016.04.008>
- DeSilva, J. M., Holt, K. G., Churchill, S. E., Carlson, K. J., Walker, C. S., Zipfel, B., & Berger, L. R. (2013). The lower limb and mechanics of walking in *Australopithecus sediba*. *Science*, 340, 1232999. <https://doi.org/10.1126/science.1232999>
- Dirks, P. H. G. M., Roberts, E. M., Hilbert-Wolf, H., Kramers, J. D., Hawks, J., Dosseto, A., ... Berger, L. R. (2017). The age of *Homo naledi* and associated sediments in the rising star cave. *South Africa. eLife*, 6, e24231. <https://doi.org/10.7554/eLife.24231>
- Domínguez-Rodrigo, M., Pickering, T. R., Baquedano, E., Mabulla, A., Mark, D. F., Musiba, C., ... Arriaza, M. C. (2013). First partial skeleton of a 1.34-million-year-old *Paranthropus boisei* from bed II, Olduvai Gorge, Tanzania. *PLoS ONE*, 8, e80347. <https://doi.org/10.1371/journal.pone.0080347>
- Garvin, H. M., Elliott, M. C., Delezene, L. K., Hawks, J., Churchill, S. E., Berger, L. R., & Holliday, T. W. (2017). Body size, brain size, and sexual dimorphism in *Homo naledi* from the Dinaledi chamber. *Journal of Human Evolution*, 111, 119–138. <https://doi.org/10.1016/j.jhevol.2017.06.010>
- Gilbert, W. H. (2008). Daka member hominid postcranial remains. In W. Gilbert & B. Asfaw (Eds.), *Homo erectus: Pleistocene evidence from the Middle Awash, Ethiopia* (Vol. 1, pp. 372–396). Berkeley: University of California Press.
- Grine, F. E., Jungers, W. L., Tobias, P. V., & Pearson, O. M. (1995). Fossil *Homo* femur from berg Aukas, northern Namibia. *American Journal of Physical Anthropology*, 97, 151–185. <https://doi.org/10.1002/ajpa.1330970207>
- Haeusler, M., & McHenry, H. M. (2004). Body proportions of *Homo habilis* reviewed. *Journal of Human Evolution*, 46, 433–465. <https://doi.org/10.1016/j.jhevol.2004.01.004>
- Haile-Selassie, Y., Latimer, B. M., Alene, M., Deino, A. L., Gibert, L., Melillo, S. M., ... Lovejoy, C. O. (2010). An early *Australopithecus afarensis* postcranium from Woranso-mille, Ethiopia. *Proceedings of the National Academy of Sciences*, 107, 12,121–12,126. <https://doi.org/10.1073/pnas.1004527107>
- Hammond, A. S., Plavcan, J. M., & Ward, C. V. (2013). Precision and accuracy of acetabular size measures in fragmentary hominin pelves obtained using sphere-fitting techniques. *American Journal of Physical Anthropology*, 150, 565–578. <https://doi.org/10.1002/ajpa.22228>
- Harcourt-Smith, W., Throckmorton, Z., Congdon, K. A., Zipfel, B., Deane, A. S., Drapeau, M. S. M., ... DeSilva, J. M. (2015). The foot of *Homo naledi*. *Nature Communications*, 6(8), 432. <https://doi.org/10.1038/ncomms9432>
- Hawks, J., Elliott, M. C., Schmid, P., Churchill, S. E., de Ruiter, D. J., Roberts, E. M., ... Berger, L. R. (2017). New fossil remains of *Homo naledi* from the Lesedi chamber South Africa. *eLife*, 6, e24232. <https://doi.org/10.7554/eLife.24232>
- Heiple, K. G., & Lovejoy, C. O. (1971). The distal femoral anatomy of *Australopithecus*. *American Journal of Physical Anthropology*, 35, 75–84. <https://doi.org/10.1002/ajpa.1330350109>
- Johanson, D. C., Lovejoy, C. O., Kimbel, W. H., White, T. D., Ward, S. C., Bush, M. E., ... Coppens, Y. (1982). Morphology of the Pliocene partial hominid skeleton (a.L. 288-1) from the Hadar formation, Ethiopia. *American Journal of Physical Anthropology*, 57, 403–451. <https://doi.org/10.1002/ajpa.1330570403>
- Jungers, W. L. (1988). Relative joint size and hominoid locomotor adaptations with implications for the evolution of hominid bipedalism. *Journal of Human Evolution*, 17, 247–265. [https://doi.org/10.1016/0047-2484\(88\)90056-5](https://doi.org/10.1016/0047-2484(88)90056-5)
- Jungers, W. L., Larson, S. G., Harcourt-Smith, W., Morwood, M. J., Sutikna, T., Due Awe, R., & Djubiantono, T. (2009). Descriptions of the lower limb skeleton of *Homo floresiensis*. *Journal of Human Evolution*, 57, 538–554. <https://doi.org/10.1016/j.jhevol.2008.08.014>
- Kennedy, G. E. (1983). A morphometric and taxonomic assessment of a hominine femur from the lower member, Koobi fora, Lake Turkana. *American Journal of Physical Anthropology*, 61, 429–436. <https://doi.org/10.1002/ajpa.1330610405>

- Kennedy, G. E. (1984). The emergence of *Homo sapiens*: The post-cranial evidence. *Man*, 19, 94–110. <https://doi.org/10.2307/2803226>
- Lordkipanidze, D., Jashashvili, T., Vekua, A., De León, M. S. P., Zollikofer, C. P. E., Rightmire, G. P., ... Rook, L. (2007). Postcranial evidence from early *Homo* from Dmanisi, Georgia. *Nature*, 449, 305–310. <https://doi.org/10.1038/nature06134>
- Lovejoy, C. O. (2007). The natural history of human gait and posture. Part 3. The knee. *Gait and Posture*, 25, 325–341. <https://doi.org/10.1016/j.gaitpost.2006.05.001>
- Lovejoy, C. O., Johanson, D. C., & Coppens, Y. (1982). Hominid lower limb bones recovered from the Hadar formation: 1974–1977 collections. *American Journal of Physical Anthropology*, 57, 679–700.
- Lovejoy, C. O., Meindl, R. S., Ohman, J. C., Heiple, K. G., & White, T. D. (2002). The Maka femur and its bearing on the antiquity of human walking: Applying contemporary concepts of morphogenesis to the human fossil record. *American Journal of Physical Anthropology*, 119, 97–133. <https://doi.org/10.1002/ajpa.10111>
- Manly, B. F. J. (2006). *Randomization, bootstrap, and Monte Carlo methods in biology* (3rd ed.). New York, NY: CRC Press.
- Marchi, D., Walker, C. S., Wei, P., Holliday, T. W., Churchill, S. E., Berger, L. R., & DeSilva, J. M. (2017). The thigh and leg of *Homo naledi*. *Journal of Human Evolution*, 104, 174–204. <https://doi.org/10.1016/j.jhevol.2016.09.005>
- McHenry, H. M. (1988). New estimates of body weight in early hominids and their significance to encephalization and megadontia in "robust" australopithecines. In F. E. Grine (Ed.), *Evolutionary history of the "robust" australopithecines* (pp. 133–148). New York: Aldine de Gruyter.
- McHenry, H. M. (1992). Body size and proportions in early hominids. *American Journal of Physical Anthropology*, 87(4), 407–431.
- Mosimann, J. E. (1970). Size allometry: Size and shape variables with characterizations of the lognormal and generalized gamma distributions. *Journal of the American Statistical Association*, 65, 930–945. <https://doi.org/10.1080/01621459.1970.10481136>
- Partridge, T. C., Granger, D. E., Caffee, M. W., & Clarke, R. J. (2003). Lower Pliocene hominid remains from Sterkfontein. *Science*, 300, 607–612. <https://doi.org/10.1126/science.1081651>
- Pickering, T. R., Heaton, J. L., Clarke, R. J., Sutton, M. B., Brain, C. K., & Kuman, K. (2012). New hominid fossils from member 1 of the Swartkrans formation, South Africa. *Journal of Human Evolution*, 62, 618–628. <https://doi.org/10.1016/j.jhevol.2012.02.003>
- Plavcan, J. M., Hammond, A. S., & Ward, C. V. (2014). Brief communication: Calculating hominin and nonhuman anthropoid femoral head diameter from acetabular size. *American Journal of Physical Anthropology*, 155(3), 469–475. <https://doi.org/10.1002/ajpa.22591>
- R Core Team. (2018). *R: A language and environment for statistical computing*. Vienna, Austria: R Foundation for Statistical Computing URL <https://www.R-project.org/>
- Reed, K. E., Kitching, J. W., Grine, F. E., Jungers, W. L., & Sokoloff, L. (1993). Proximal femur of *Australopithecus africanus* from member 4, Makapansgat, South Africa. *American Journal of Physical Anthropology*, 92, 1–15. <https://doi.org/10.1002/ajpa.1330920102>
- Richmond, B. G., & Jungers, W. L. (1995). Size variation and sexual dimorphism in *Australopithecus afarensis* and living hominoids. *Journal of Human Evolution*, 29, 229–245.
- Richmond, B. G., & Jungers, W. L. (2008). *Orrorin tugenensis* femoral morphology and the evolution of hominin bipedalism. *Science*, 319, 1662–1665. <https://doi.org/10.1126/science.1154197>
- Ruff, C. B. (1995). Biomechanics of the hip and birth in early *Homo*. *American Journal of Physical Anthropology*, 98, 527–574. <https://doi.org/10.1002/ajpa.1330980412>
- Ruff, C. B. (2010). Body size and body shape in early hominins - implications of the Gona pelvis. *Journal of Human Evolution*, 58, 166–178. <https://doi.org/10.1016/j.jhevol.2009.10.003>
- Ruff, C. B., Puymeraul, L., Macchiarelli, R., Sipla, J., & Ciochon, R. L. (2015). Structure and composition of the Trinil femora: Functional and taxonomic implications. *Journal of Human Evolution*, 80, 147–158. <https://doi.org/10.1016/j.jhevol.2014.12.004>
- Sokal, R. R., & Rohlf, F. J. (1995). *Biometry* (3rd ed.). New York, NY: W.H. Freeman and Company.
- Sutikna, T., Tocheri, M. W., Morwood, M. J., Saptomo, E. W., Jatmiko, A., Due, R., ... Roberts, R. G. (2016). Revised stratigraphy and chronology for *Homo floresiensis* at Liang Bua in Indonesia. *Nature*, 532, 366–369. <https://doi.org/10.1038/nature17179>
- Tardieu, C. (2010). Development of the human hind limb and its importance for the evolution of bipedalism. *Evolutionary Anthropology: Issues, News, and Reviews*, 19, 174–186. <https://doi.org/10.1002/evan.20276>
- ThermoFisher Scientific. 2017. Amira 6.4 [Computer software].
- Trinkaus, E., & Ruff, C. B. (1999). Diaphyseal cross-sectional geometry of near eastern middle Paleolithic humans: The femur. *Journal of Archaeological Science*, 26, 409–424. <https://doi.org/10.1006/jasc.1998.0343>
- Walker, A., & Leakey, R. (1993). The postcranial bones. In A. Walker & R. Leakey (Eds.), *The Nariokotome Homo erectus skeleton* (pp. 95–160). Cambridge, MA: Harvard University Press. <https://doi.org/10.1016/0169-5347>
- Ward, C. V., Feibel, C. S., Hammond, A. S., Leakey, L. N., Moffett, E. A., Plavcan, J. M., ... Leakey, M. G. (2015). Associated ilium and femur from Koobi fora, Kenya, and postcranial diversity in early *Homo*. *Journal of Human Evolution*, 81, 48–67. <https://doi.org/10.1016/j.jhevol.2015.01.005>
- Ward, C. V., Kimbel, W. H., Harmon, E. H., & Johanson, D. C. (2012). New postcranial fossils of *Australopithecus afarensis* from Hadar, Ethiopia (1990–2007). *Journal of Human Evolution*, 63, 1–51. <https://doi.org/10.1016/j.jhevol.2011.11.012>

## SUPPORTING INFORMATION

Additional supporting information may be found online in the Supporting Information section at the end of this article.

**How to cite this article:** Walker CS, Cofran ZD, Grabowski M, et al. Morphology of the *Homo naledi* femora from Lesedi. *Am J Phys Anthropol*. 2019;1–19. <https://doi.org/10.1002/ajpa.23877>